

Colour Octet Contribution in Exclusive P-Wave Charmonium Decay into Octet and Decuplet Baryons

S.M.H. Wong

*School of Physics and Astronomy, University of Minnesota, Minneapolis,
MN 55455, USA¹*

Fachbereich Physik, Universität Wuppertal, D-42097 Wuppertal, Germany

*Institute of Accelerating Systems and Applications (IASA), P.O. Box 17214,
GR-10024 Athens, Greece*

and

*Nuclear and Particle Physics Section, University of Athens, Panepistimiopolis,
GR-15771 Athens, Greece*

Abstract

In the last years, the need of the colour octet state in inclusive P-wave charmonium decay has been firmly established. However, the implications of this in the corresponding exclusive reactions have not been fully recognized. We argue for the necessity of the colour octet in P- and higher-wave quarkonium decay. Using a set of phenomenologically constructed baryon wavefunctions, we consider the χ_J decay into octet and decuplet baryon-antibaryon pair. By doing so, we subject the wavefunctions to a test of applicability. We show that the colour singlet component alone is insufficient to account for experimental measurements and only by including the colour octet contribution can the partial theoretical decay widths be brought into range of the data. By the present and earlier applications of the set of wavefunctions, they show themselves to be reasonable model wavefunctions at around the scale $Q^2 \sim 10\text{-}20 \text{ GeV}^2$.

¹present address

1 Introduction

In studying strong interactions exclusive processes, a more reliable method is one that bases on perturbative QCD, which calls to mind the likes of deep inelastic scattering. However unlike in these inclusive reactions where the final states of hadrons can be summed over so no explicit knowledge of any of the hadrons is required, in exclusive processes one is usually interested specifically only in a few final hadrons at a time, as such the knowledge of the wavefunctions of these hadrons is essential. The more accurate picture of a hadron is the Fock state expansion where it is seen as a sum of states with increasing number of constituents starting from the state with only the valence quarks and/or antiquarks. The probability of the hadron being in any of these states is given by the modulus squared of the wavefunction associated with each of these states.

$$\begin{aligned}
 |B\rangle &= \psi_{\text{valence}}|q_1^v q_2^v q_3^v\rangle + \psi_g|q_1^v q_2^v q_3^v g\rangle + \psi_q|q_1^v q_2^v q_3^v q\bar{q}\rangle + \dots \\
 &\quad + \psi_{g_1\dots g_M q_1\dots q_N}|q_1^v q_2^v q_3^v g_1 \dots g_M q_1 \bar{q}_1 \dots q_N \bar{q}_N\rangle + \dots \\
 |M\rangle &= \psi_{\text{valence}}|q_1^v \bar{q}_2^v\rangle + \psi_g|q_1^v \bar{q}_2^v g\rangle + \psi_q|q_1^v \bar{q}_2^v q\bar{q}\rangle + \dots \\
 &\quad + \psi_{g_1\dots g_M q_1\dots q_N}|q_1^v \bar{q}_2^v g_1 \dots g_M q_1 \bar{q}_1 \dots q_N \bar{q}_N\rangle + \dots
 \end{aligned}$$

Because the number of constituents is unlimited, one would require, in general, far too much information before an exclusive process involving even just a few hadrons can be studied. Fortunately as shown by Brodsky and Lepage in ref. [1] in the so-called standard hard scattering approach (SHSA), when a high momentum transfer or high Q^2 is involved in an exclusive process, not only is there factorization and so the process can be partially calculated perturbatively, but also only the lowest valence Fock state wavefunctions of the hadrons are needed. The higher Fock states are suppressed by the large Q^2 . Thus the large momentum transfer acts as a filter to let past only the lowest state of the hadrons. It has also been proved by Duncan and Mueller [2] that these are also true in quarkonium decay with large timelike momentum transfer.

Most recent developments in inclusive quarkonium physics have seen, on the other hand, the need of the next higher Fock state in P-wave quarkonia [3, 4], the so-called colour octet, where the heavy $Q\bar{Q}$ pair is in a colour octet rather than the usual colour singlet as in the valence state. This higher state is made up of the $Q\bar{Q}$ plus a gluon. This is special to heavy quarkonium and can be understood in terms of a suppression on the level of the wavefunction due to angular momentum as we will explain in later sections. The advance in inclusive process involving quarkonia has yet to fully bring about the same level of understanding in the corresponding exclusive process. Part of our goal in this paper is therefore to show that colour octet is not only important in inclusive but also in exclusive process. We will achieve this by studying the P-wave χ_J decay into baryon-antibaryon.

As mentioned above, knowledge of hadronic wavefunctions is very important. Even in large momentum transfer processes, valence wavefunctions are still necessary. Since

bound state wave equations in QCD are too hard to solve, other ways to obtain the solutions or the hadronic wavefunctions must be used. One way is via QCD moment sum rules [5, 6, 7]. However, it has been shown in [8] that perturbative calculation of the proton magnetic form factor using a range of existing nucleon distribution amplitudes so-obtained gives results that are, on the average, at least a factor of two below experimental measurements in the range of Q^2 up to 50 GeV². It is therefore clear that perturbative contribution is not dominant in this rather low range of Q^2 . The same conclusion has also been pointed out in [9]. Nucleon wavefunctions constructed from such distribution amplitudes are, therefore not applicable in reactions with far from asymptotic values of Q^2 , not to mention the fact that there might be ambiguities in the distribution amplitudes determined this way.

In order to obtain a nucleon wavefunction that is suitable for application at as low as 10 GeV². The usually neglected but nevertheless ever present soft overlap between the final and initial nucleon wavefunction contribution to the magnetic form factor is taken to make up for the difference between the perturbative contribution and the experimental measurements. It was shown in [10] that a nucleon model wavefunction could indeed be constructed this way, using constraints from valence quark distribution, J/ψ decay width into nucleon-antinucleon pair and existing data on nucleon electromagnetic form factor. Our motivation in this regard is to show that the above construction of a model nucleon wavefunction and its generalization to other octet and decuplet baryons [11] provide a reasonable description of the baryonic valence Fock state wavefunctions at around 10 GeV². To do that we must apply these wavefunctions to exclusive processes. Our investigation will allow us to study this as well as the colour octet contribution.

Since in χ_J decay into baryon-antibaryon, only nucleon-antinucleon in the final state has been measured, our calculations will show first that colour singlet contribution alone is not sufficient and by including that of the octet, the partial decay width can be brought into reasonable agreement with experiment. Then with the generalization of the nucleon wavefunction to the whole flavour octet and decuplet multiplet, we can provide predictions for the widths of χ_J decay into other baryon pairs.

The paper is organized as follows. First we review briefly in Sec. 2 the angular momentum suppression in the P-wave wavefunction and in Sec. 3 give theoretical argument for the inclusion of the colour octet component in exclusive decay process. In Sec. 4, the set of phenomenologically constructed baryon wavefunctions will be presented and explained before we use the improved modified hard scattering scheme (MHSA) of Botts, Li and Serman [12, 13] to obtain the singlet contribution in Sec. 5 and 6. The results will be compared to experiment. In Sec. 7, our method in obtaining a wavefunction of the higher colour octet state of the χ_J and the Feynman graphs of the decay process will be given. The details in constructing the octet contribution to the hard perturbative part T_H will be explained in Sec. 8. The actual calculation and the results are in Sec. 9 and 10, respectively. In the appendices, all essential details of the calculation, the propagators and the numerators of the graphs used in Sec. 9 are given.

2 Angular Momentum Suppression Of Charmonium Wavefunctions

In this section, we show that there is a suppression on the charmonium wavefunction due simply to the angular momentum of the heavy quark-antiquark system. This has important consequences as we will see in the next section, where we briefly review the more detailed argument given in [14]. Hadronic decay of charmonium is through the annihilation of the charm with the anticharm, which is a short distance process because of the heavy charmonium mass. The annihilation size L is roughly given by $L \sim 1/M$, the inverse of the heavy mass M . The charmonium wavefunction, which must enter the decay probability amplitude, is therefore needed predominantly at $L \sim 1/M \sim 0$ for a heavy charmonium decay. That is $\psi_S(L) \sim \psi_S(0)$, the wavefunction at the spatial origin. This is the case for S-wave charmonium such as η_c or J/ψ . For a P-wave charmonium, the wavefunction in fact vanishes at the origin, so instead one has to expand the wavefunction around the origin. What enters the probability amplitude is actually $\psi_P(L) \sim L\psi'_P(L) \sim L\psi'_P(0)$. Going to momentum space, the probability amplitudes for a S- and P-wave decay include the wavefunction of the form

$$\begin{aligned} \text{S-wave:} \quad & \psi_S(L) \quad \longrightarrow \tilde{\psi}_S(k) \\ \text{P-wave:} \quad & \psi_P(L) \sim L\psi'_P(0) \longrightarrow \frac{k}{M}\tilde{\psi}_P(k) , \end{aligned}$$

respectively, where k is the internal momentum of the charmonium, the average value $\langle k \rangle$ is of the order of a few hundreds MeV. So it becomes clear that P-wave decay is suppressed by $1/M$ in comparison to S-wave at the level of the wavefunction. This suppression is one of the reasons why colour octet is necessary for a P-wave inclusive decay. We will see in the next section that it also provides the reason for its inclusion in exclusive decays.

3 Comparison Of The Large Scale Dependence Of Colour Singlet and colour octet

The simplest scheme to calculate charmonium partial decay width that is built on the solid basis of perturbative QCD is the hard scattering approach of Brodsky and Lepage [1]. In this scheme, decay probability amplitude can be factorized into hard and soft part and is given by a convolution of hadronic distribution amplitudes ϕ 's and the hard perturbative part T_H . For the decay of χ_J into baryon-antibaryon, or more specifically nucleon-antinucleon, this is

$$\mathcal{M} \sim f_{\chi_J}\phi_{\chi_J}(x) \otimes f_N\phi_N(x) \otimes f_{\bar{N}}\phi_{\bar{N}}(x) \otimes T_H(x) . \quad (1)$$

Since the distribution amplitudes are nothing but the hadronic wavefunctions with their internal transverse momenta being integrated over, there is still the decay constant f

accompanying each distribution amplitude. While the amplitude themselves are dimensionless, the decay constants f 's carry different mass dimensions depending on the original hadronic wavefunctions. From the fact that the partial decay width is given by

$$\Gamma_{\text{partial}} \sim |\mathcal{M}|^2/M \quad (2)$$

and there is only one mass scale M in the process, namely the heavy charmonium mass, we can use power counting on Eq. (1) to compare, once the mass dimensions of the decay constants are known, the colour singlet and octet contribution to the decay width and hence their relative importance to a particular hadronic decay process. For the determination of the mass dimension of f , we refer to [14].

Examining Eq. (1), the decay constant of the valence Fock state of nucleon f_N and the colour octet charmonium decay constant $f_{\chi_J}^{(8)}$ are both 3-particle wavefunction. Therefore they must be of mass dimension two. The colour singlet decay constant $f_{\chi_J}^{(1)}$, on the other hand, is a 2-particle wavefunction so it should be of dimension one. However, the fact that χ_J are P-wave charmonia increases this to dimension two. The only remaining quantity in Eq. (1) that has a dimension is T_H , which contains a hidden power of M . This power must make up the right dimension for \mathcal{M} , which must be dimension one in view of Eq. (2). So we can now collect all the dimensional quantities in the colour singlet and octet probability amplitude and determine their dependence on the large scale M . We get

$$\mathcal{M}^{(1)} \sim M \frac{f_{\chi_J}^{(1)}}{M^2} \left(\frac{f_N}{M^2} \right)^2 \sim \frac{1}{M^5} \quad (3)$$

$$\mathcal{M}^{(8)} \sim M \frac{f_{\chi_J}^{(8)}}{M^2} \left(\frac{f_N}{M^2} \right)^2 \sim \frac{1}{M^5}. \quad (4)$$

It is now clear that both the singlet and octet contribution for the P-wave χ_J are weighed by the inverse fifth power of the charmonium mass. The colour octet, although a higher Fock state of the charmonium, is not suppressed by the large scale of the decay process in relation to the valence singlet state.

If there were no suppression at the level of the P-wave wavefunction as explained in the previous section, for example in the case of J/ψ decay, the dependence of the singlet contribution on M would have been $1/M^4$. Therefore the colour octet contribution can be neglected in the decay of a S-wave but not that of a P-wave charmonium. For more details of the argument above, one can consult [14].

4 Baryon Wavefunctions

4.1 Octet Baryons

As mentioned in Sec. 1, most model wavefunctions constructed from QCD moment sum rules [5, 6, 7, 15, 16, 17] lead to rather unsatisfactory distribution amplitudes at mod-

erate Q^2 [8, 9] and they certainly do not describe experimental data. A different model wavefunction suitable for application at such low momentum transfers was constructed in [10]. This construction is based on the following form of the nucleon wavefunction,

$$|p, +\rangle = \frac{\varepsilon_{a_1 a_2 a_3}}{\sqrt{3!}} \int [dx][d^2\mathbf{k}_\perp] \left\{ \Psi_{123}^N |u_+^{a_1} u_-^{a_2} d_+^{a_3}\rangle + \Psi_{213}^N |u_-^{a_1} u_+^{a_2} d_+^{a_3}\rangle \right. \\ \left. - (\Psi_{132}^N + \Psi_{231}^N) |u_+^{a_1} u_+^{a_2} d_-^{a_3}\rangle \right\} \quad (5)$$

which is the most general of the nucleon wavefunction with zero orbital angular momentum [18]. The nucleon, being an isospin doublet, is also the lowest energy state of the baryons and is therefore reasonable for one to assume that it has zero orbital angular momentum. These conditions permit the presence of only one scalar function Ψ , which is a function of the light-cone momentum fractions x_i and the internal transverse momentum $\mathbf{k}_{\perp i}$ of the nucleon. In the notations of [10], it is given in terms of the nucleon decay constant, or equivalently the wavefunction at the origin f_N , the distribution amplitude ϕ_{123} and the function containing the transverse momentum dependence Ω_N , by

$$\Psi_{123}(x, \mathbf{k}_\perp) = \Psi(x_1, x_2, x_3; \mathbf{k}_{\perp 1}, \mathbf{k}_{\perp 2}, \mathbf{k}_{\perp 3}) = \frac{1}{8\sqrt{3!}} f_N(\mu_F) \phi_{123}^N(x, \mu_F) \Omega_N(x, \mathbf{k}_\perp). \quad (6)$$

and

$$[dx] = \prod_{i=1}^3 dx_i \delta(1 - \sum_{i=1}^3 x_i) \quad [d^2\mathbf{k}_\perp] = \frac{1}{(16\pi^3)^2} \prod_{i=1}^3 d^2\mathbf{k}_{\perp i} \delta^{(2)}(\sum_{i=1}^3 \mathbf{k}_{\perp i}). \quad (7)$$

are the usual constrained integration measures over momentum fractions and the internal transverse momenta. The function Ω_N is conveniently taken to be of Gaussian form

$$\Omega_N(x, \mathbf{k}_\perp) = (16\pi^2)^2 \frac{a_N^4}{x_1 x_2 x_3} \exp \left[-a_N^2 \sum_{i=1}^3 \mathbf{k}_{\perp i}^2 / x_i \right]. \quad (8)$$

where a_N is a transverse size parameter which was fitted together with the decay constant f_N to experimental data by the procedure described in [10] to be $a_N = 0.75 \text{ GeV}^{-1}$ and $f_N(\mu_0) = 6.64 \times 10^{-3} \text{ GeV}^2$ at the reference scale $\mu_0 = 1.0 \text{ GeV}$.

The distribution amplitude ϕ_{123} as well as the decay constant, all have to be evolved to the factorization scale μ_F of the process in question. In terms of the eigenstates of the evolution equation, the effect of the evolution is to change the coefficients of each eigenstate by a certain power of the log of the relevant scale. The nucleon distribution amplitude expressed in the Appell polynomial eigenbasis is

$$\phi_{123}^N(x, \mu_F) = \phi_{\text{AS}}(x) \left[1 + \sum_{n=1}^{\infty} B_n^N(\mu_F) \tilde{\phi}_{123}^n(x, \mu_F) \right] \quad (9)$$

$$= \phi_{\text{AS}}(x) \left[1 + \frac{3}{4} \tilde{\phi}_{123}^1(x) + \frac{1}{4} \tilde{\phi}_{123}^2(x) \right] = 60x_1 x_2 x_3 [1 + 3x_1]. \quad (10)$$

Under a change of scale both the coefficients B_n^N of the expansion and the decay constant are scaled by the following factors of logarithm of the relevant scale μ_F

$$f_N(\mu_F) = f_N(\mu_0) \left(\frac{\ln(\mu_0/\Lambda_{\text{QCD}})}{\ln(\mu_F/\Lambda_{\text{QCD}})} \right)^{2/3\beta_0}, B_n^N(\mu_F) = B_n^N(\mu_0) \left(\frac{\ln(\mu_0/\Lambda_{\text{QCD}})}{\ln(\mu_F/\Lambda_{\text{QCD}})} \right)^{\tilde{\gamma}_n/\beta_0} \quad (11)$$

where $\tilde{\gamma}_n$ are the reduced anomalous dimensions and β_0 is the first coefficient of the β function. The last line in Eq. (10) is the expression for ϕ_{123}^N at the scale $\mu_F = \mu_0$.

As shown in [11], the form of the nucleon wave function need not be restricted to the SU(2) isospin doublet. On the contrary, one can extend it to the complete SU(3) flavour octet. The simplest way to do this, with SU(3) flavour symmetry breaking by the heavier strange quark mass taken into account, is to assume the complete baryon octet shares the same octet transverse size parameter, $a_{B_8} = 0.75$ GeV and the octet decay constant, $f_{B_8} = 6.64 \times 10^{-3}$ GeV². Then the flavour symmetry breaking effects are all put into the octet distribution amplitudes $\phi_{123}^{B_8}$ and they manifest themselves as uneven distribution of the light-cone momentum fractions amongst the valence quarks. As shown in [11], introducing an additional exponential dependence on the strange constituent quark mass m_s , of the form

$$\exp\left(-\frac{a_{B_8}^2 m_s^2}{x_j}\right) \quad (12)$$

in the distribution amplitude for each strange quark with label j suffices for the purpose. Using several different values of m_s , representative sets of the expansion coefficients B^{B_8} , of the octet distribution amplitudes, $\phi_{123}^{B_8}$ can be obtained. The set 3 in [11], obtained with $m_s = 350$ MeV, shows the most promise and will be used in the following investigations.

The octet baryon wavefunctions with positive helicities can then be expressed as follows.

$$|B_8, +\rangle = \frac{\varepsilon_{a_1 a_2 a_3}}{\sqrt{3!}} \int [dx][d^2\mathbf{k}_\perp] \left\{ \Psi_{123}^{B_8} |f_{1+}^{a_1} f_{1-}^{a_2} f_{2+}^{a_3}\rangle + \Psi_{213}^{B_8} |f_{1-}^{a_1} f_{1+}^{a_2} f_{2+}^{a_3}\rangle \right. \\ \left. - \left(\Psi_{132}^{B_8} + \Psi_{231}^{B_8} \right) |f_{1+}^{a_1} f_{1+}^{a_2} f_{2-}^{a_3}\rangle \right\}, \quad (13)$$

$$|\Lambda, +\rangle = \frac{\varepsilon_{a_1 a_2 a_3}}{\sqrt{2}} \int [dx][d^2\mathbf{k}_\perp] \left\{ \Psi_{123}^\Lambda |u_+^{a_1} d_-^{a_2} s_+^{a_3}\rangle - \Psi_{213}^\Lambda |u_-^{a_1} d_+^{a_2} s_+^{a_3}\rangle \right. \\ \left. + \left(\Psi_{132}^\Lambda - \Psi_{231}^\Lambda \right) |u_+^{a_1} d_+^{a_2} s_-^{a_3}\rangle \right\}, \quad (14)$$

where $f_j^{a_i}$ stands for the quark flavour of quark j with colour a_i and $\Psi_{123}^{B_8}$ is the corresponding scalar functions in Eq. (6) of the octet baryons. The Λ is a slightly different member of the flavour octet multiplet. Being an isospin singlet, it has to vanish under the action of $\text{SU}(2)_{\text{isospin}}$ and therefore has different signs between the different wavefunction components.

4.2 Decuplet Baryons

As we mentioned in the introduction, our interest in this investigation is the χ_J decay into baryon-antibaryon pair. Unlike the octet baryon-antibaryon which can coupled only to spin $S=1$, a decuplet baryon-antibaryon pair can coupled to $S=2$ as well. This leads to the interesting potential possibility of χ_2 with $S_z = 2$ to decay into a coupled decuplet baryon pair with the same total third component of the spin. However within perturbative QCD, this is not possible due to quark and gluon couple via a vector coupling. This results in the well known helicity conservation or helicity sum rule, which forces the outgoing baryon-antibaryon to have zero total helicity [19]. Or in other words, they must be in a total spin one state. For the same reason, χ_0 decay into baryon-antibaryon is forbidden. Therefore for the decuplet baryons, all we need are the helicity +1 decuplet baryon wavefunctions.

Starting from the Δ^{++} , the simplest distribution amplitude which is symmetric between the three u-quarks is the asymptotic distribution amplitude $\phi_{AS}(x)$. Using this as the starting point, one can likewise generalized to the whole decuplet baryon multiplet and introduce SU(3) flavour symmetry breaking in the same manner as in Sec. 4.1 by using an exponential m_s dependence. This again yields several sets of representative expansion coefficients $B_n^{B_{10}}$, for the decuplet baryon distribution amplitudes $\phi_{123}^{B_{10}}(x)$. They are listed in Table 1. The decuplet wavefunctions can be expressed in a similar fashion as before

$$\begin{aligned}
 |\Delta^{++}, +\rangle &= \frac{\varepsilon_{a_1 a_2 a_3}}{\sqrt{2}} \int [dx][d^2\mathbf{k}_\perp] \Psi_{123}^\Delta |u_+^{a_1} u_+^{a_2} u_+^{a_3}\rangle \\
 |B_{10}, +\rangle &= \frac{\varepsilon_{a_1 a_2 a_3}}{\sqrt{3!}} \int [dx][d^2\mathbf{k}_\perp] \left\{ \Psi_{123}^{B_{10}} |f_{1+}^{a_1} f_{1-}^{a_2} f_{2+}^{a_3}\rangle + \Psi_{213}^{B_{10}} |f_{1-}^{a_1} f_{1+}^{a_2} f_{2+}^{a_3}\rangle \right. \\
 &\quad \left. + \Psi_{132}^{B_{10}} |f_{1+}^{a_1} f_{1+}^{a_2} f_{2-}^{a_3}\rangle \right\}. \quad (16)
 \end{aligned}$$

and now the scalar functions are

$$\Psi_{123}^{B_{10}}(x, \mathbf{k}_\perp) = \frac{f_{B_{10}}(\mu_F)}{24\sqrt{2}} \phi_{123}^{B_{10}}(x, \mu_F) \Omega_{B_{10}}(x, \mathbf{k}_\perp). \quad (17)$$

As shown in [11], using the assumption that the nucleon and the delta have the same valence Fock state probabilities, the decuplet decay constant and the transverse size parameter can take a range of values. We take as representative values $f_{B_{10}}(\mu_0) = 0.0143 \text{ GeV}^2$ and $a_{B_{10}} = 0.80 \text{ GeV}^{-1}$.

5 χ_J Decay In The Modified Hard Scattering Approach

Since the χ_0 decay into baryon-antibaryon is forbidden by angular momentum conservation and the not-yet-confirmed 1P_1 state h_c cannot preserve C-parity and parity simultaneously in this decay mode [22] in a perturbative approach, only χ_1 and χ_2 may have

	B_1	B_2	B_3	B_4	B_5
Δ	0.000	0.000	0.000	0.000	0.000
Σ^*	-0.547	0.182	-0.216	-1.081	0.062
Ξ^*	0.540	-0.180	-0.382	1.742	-0.413

Table 1: The expansion coefficients of the distribution amplitudes $\phi_{123}^{B_{10}}$ of the octet baryons considered in the χ_J decay. The parameters associated with this set of coefficients are $f_{B_{10}}(\mu_0) = 0.0143 \text{ GeV}^2$ and $a_{B_{10}} = 0.80 \text{ GeV}^{-1}$.

finite partial decay widths ² into baryon-antibaryon pair. The helicity amplitudes in covariant form in terms of the baryon-antibaryon spinors $u_B(p, \lambda)$ and $v_B(p, \lambda)$ suitable for our consideration are, for χ_1

$$\mathcal{M}_{\lambda_1 \lambda_2 \lambda}^1 = \bar{u}_B(p_1, \lambda_1) \mathcal{B}_1 \gamma^\nu v_B(p_2, \lambda_2) \epsilon_\nu(\lambda), \quad (18)$$

and for χ_2

$$\mathcal{M}_{\lambda_1 \lambda_2 \lambda}^2 = \bar{u}_B(p_1, \lambda_1) \mathcal{B}_2 \gamma^\nu v_B(p_2, \lambda_2) \epsilon_{\mu\nu}(\lambda) \frac{(p_2^\mu - p_1^\mu)}{M_{\chi_2}}, \quad (19)$$

where ϵ_μ and $\epsilon_{\mu\nu}$ are the polarization vector and tensor of χ_1 and χ_2 , respectively and \mathcal{B}_J are their corresponding decay form factors. Note that Eq. (18) and Eq. (19) are the only covariant form permitted for the corresponding helicity amplitudes. Using only γ^μ , $(p_2 - p_1)^\mu$ and $g^{\mu\nu}$ to form a vector and a symmetric tensor, they are the only form that can be constructed which still respect helicity conservation. The decay widths into baryon-antibaryon are therefore

$$\Gamma(\chi_1 \rightarrow B\bar{B}) = \frac{\rho_{\text{p.s.}}(M_B/M_{\chi_1})}{16\pi M_{\chi_1}} \frac{1}{3} \sum_{\lambda_s} |\mathcal{M}_{\lambda_1 \lambda_2 \lambda}^1|^2 = \frac{\rho_{\text{p.s.}}(M_B/M_{\chi_1}) m_c^2}{3\pi M_{\chi_1}} |\mathcal{B}_1^B|^2, \quad (20)$$

and

$$\Gamma(\chi_2 \rightarrow B\bar{B}) = \frac{\rho_{\text{p.s.}}(M_B/M_{\chi_2})}{16\pi M_{\chi_2}} \frac{1}{5} \sum_{\lambda_s} |\mathcal{M}_{\lambda_1 \lambda_2 \lambda}^2|^2 = \frac{\rho_{\text{p.s.}}(M_B/M_{\chi_2}) m_c^2}{10\pi M_{\chi_2}} |\mathcal{B}_2^B|^2. \quad (21)$$

Since in the standard or modified hard scattering scheme, baryons are treated as massless in comparison to the large scale M of the process, phase space must be corrected. This is taken care of by the phase space factor in the above equations given by $\rho_{\text{p.s.}}(z) = \sqrt{1 - 4z^2}$.

Within the SHSA, one has factorization by which the soft infrared physics is contained in the light-cone wavefunctions and a perturbatively calculable hard scattering amplitude

²In practice, χ_0 has a surprisingly large upper bound on the partial width of the decay channel in question [23] and the h_c may also have non-zero partial decay width. This should be attributed to non-perturbative soft physics or higher twist effects since mass corrections alone should not yield such large width assuming that the experimental width is near the upper limit.

T_H . In the present problem, the hard scale is set by twice the charm quark mass $2m_c$, rather than by the charmonium mass M_{χ_J} , because as we mentioned before, the $c\bar{c}$ pair annihilates at a much smaller size than that of the charmonium. This explains the appearance of m_c^2 in Eq. (20) and Eq. (21). The decay amplitudes or equivalently, the decay form factors \mathcal{B}^J are expressed as a convolution of the hadron wavefunctions and the hard scattering amplitude T_H . Based on this approach, there are already a number of work on charmonium decay into nucleon-antinucleon [24, 25, 26, 27]. However, we consider these as incomplete for the following reasons. First, they used a number of nucleon wavefunctions, which did not describe the correct physics at the scale of the order of M_{χ_J} . As shown in [8], none of these wavefunctions are able to describe data of the nucleon magnetic form factor. Second, their treatments of α_s are ambiguous given that the decay widths depend on α_s^6 , any small changes in the value of α_s used will change the width considerably. It is therefore not difficult to obtain a width that match the experimental decay widths. All one has to do is to choose the right value of α_s . This is very arbitrary in our opinion. A better way is to determine the scale at which α_s should be evaluated by using the virtualities of the internal exchanged gluons. However, these virtualities in the SHSA depend on the light-cone momentum fractions. One will encounter problems as the end point regions is approached when some of these gluon virtualities drop down to Λ_{QCD}^2 . α_s will become large and the perturbative part of the SHSA breaks down. Other treatment of this problem such as arbitrarily freezing α_s at some values as the virtualities become small or using an equally arbitrary gluon mass is not well justified. Third, as we have already discussed due to the development first shown in [3, 4] that the contributions from the next higher Fock state of the P-wave charmonium, where the $c\bar{c}$ pair is in a colour octet, are comparable to that of the lowest colour singlet contribution because of suppression by angular momentum. To the best of our knowledge, colour octet contributions have not been taken into account in most exclusive reaction involving P- and higher wave charmonium. In the case of the decay into light pseudoscalar mesons, this has been worked out recently within the SHSA in [20] and within the MHSA in [21].

To deal with the above deficiencies of the previous calculations, the phenomenologically constructed nucleon wavefunction and its generalization to the whole of the octet and decuplet baryon multiplets [10, 11] should provide better baryon wavefunctions at around 10 GeV². The problem with the coupling can be dealt with successfully with the MHSA although it complicates the calculation with the additional, but necessary transverse momentum dependence for a self-consistent description. The above mentioned end point problem in which one runs into the infrared non-perturbative region within a perturbative scheme is cured by the introduction of radiative corrections in the form of Sudakov factor which spans the energy range between the lower factorization scale μ_F and the higher hard scale of the process in question. The Sudakov factor with transverse size dependence was first calculated in [12, 13] and was shown to cure the problem in the case of the pseudoscalar meson scattering. In the case of baryons, this will provide a cure of the above problem only if one supplements the Sudakov suppression factor with the

MAX prescription for deciding the infrared cutoff scale [8]. This amounts to choosing the largest transverse separation scale as the infrared cutoff, which is physical in the sense that very long wavelength gluons cannot resolve a “small” hadron which is colour singlet as far as the gluon is concerned.

6 Colour Singlet Contribution

P-wave charmonium decays dominantly through annihilation into gluons, which is a short distance process set by the scale of the charmonium mass M_{χ_J} . The non-perturbative information of the bounded system must come from and be parametrized by the wavefunction of the χ_J at small spatial separation, usually taken to be at the origin. For P-wave charmonium, the vanishing of the wavefunction at the origin forces the substitution of the wavefunction there by the first derivative of the radial wavefunction

$$R'_P(0) = \frac{4i\sqrt{\pi m_c}}{3\sqrt{3}} \int \frac{d^3\mathbf{k} k^2}{(2\pi)^3 2M_{\chi_{J=1,2}}} \tilde{\Psi}_{J=1,2}^{(1)}(k) = i\sqrt{\frac{16\pi m_c}{3}} f_{\chi_{J=1,2}}^{(1)}, \quad (22)$$

where $|R'_P(0)| = 0.22 \text{ GeV}^{5/2}$ and $\Psi_{J=1,2}^{(1)}(k)$ are functions of the internal relative momentum of the $c\bar{c}$ system and are the reduced wavefunctions of the χ_J , that means a power of k has been extracted and put into the covariant spin part of the χ_J wavefunctions. This is the form of the wavefunction commonly used for χ_J . The related but more general form of the colour singlet wavefunctions of the χ_J for $J = 1, 2$ are

$$|\chi_1^{(1)}, p\rangle = \frac{\delta_{ab}}{\sqrt{3}} \int \frac{d^3\mathbf{k}}{(2\pi)^3 2M_{\chi_1}} \tilde{\Psi}_1^{(1)}(k) S_1^{(1)}(p, k) |c\bar{c}; k, p\rangle, \quad (23)$$

$$|\chi_2^{(1)}, p\rangle = \frac{\delta_{ab}}{\sqrt{3}} \int \frac{d^3\mathbf{k}}{(2\pi)^3 2M_{\chi_2}} \tilde{\Psi}_2^{(1)}(k) S_2^{(1)}(p, k) |c\bar{c}; k, p\rangle, \quad (24)$$

and the covariant spin wave function of χ_1 and χ_2 expanded up to $O(k^2)$ are

$$S_1^{(1)}(p, k) = \frac{-i}{2M_{\chi_1}} \left[\not{p} + M_{\chi_1} - \frac{2}{M_{\chi_1}} \not{p} \not{K} \right] \epsilon_{\mu\nu\alpha\beta} p^\mu \epsilon^\nu K^\alpha \gamma^\beta \quad (25)$$

$$S_2^{(1)}(p, k) = \frac{1}{\sqrt{2}} \left[(\not{p} + M_{\chi_2}) \gamma_\mu + \frac{2}{M_{\chi_2}} [(\not{p} + M_{\chi_2}) K_\mu - \not{p} \not{K} \gamma_\mu] \right] \epsilon^{\mu\nu} K_\nu, \quad (26)$$

where $K \cdot p = 0$. The δ_{ab} in the above equations is to ensure the $c\bar{c}$ is indeed in a colour singlet state.

Since χ_J are even under charge conjugation, they can annihilate into two or three gluons at leading order $O(\alpha_s^3)$ [28]. The possible types of diagrams for $c\bar{c}$ annihilation into three light quark-antiquark pairs are shown in Fig. 1. As discussed in [28], a colour singlet quark-antiquark system has C-parity $(-1)^{L+S}$, so P-wave spin-1 charmonia are all even

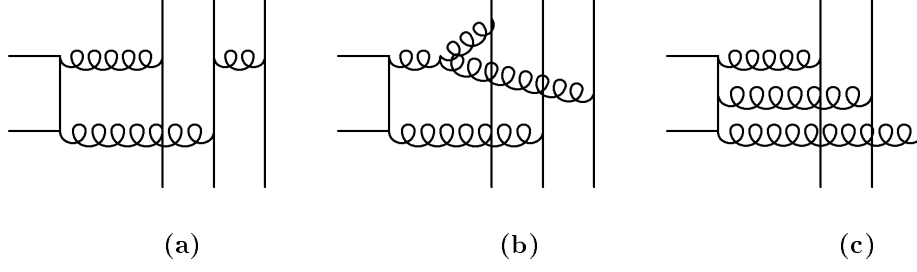


Figure 1: Basic graphs that could contribute to χ_J colour singlet decay. But actually, only graphs of type (a) can contribute.

C-parity states. Since strong interactions respect C-parity conservation, the intermediate two or three gluons must also be even under charge conjugation. Two gluons in a colour singlet state is automatically in an even C-parity state so Fig. 1(a) and (b) are possible at the two gluon stage. However in colour space, an examination of the colour structure of the baryon wavefunctions Eq. (13) and Eq. (16) show that exchanges between any two quark lines are symmetric but in Fig. 1 (b) there is an antisymmetric three-gluon coupling so it is eliminated. For the decay via three gluons in Fig. 1 (c), it is possible for three gluons to be even under C-parity through a f^{abc} coupling, but again symmetry in colour space between the three light quark lines forces the three gluons to couple via d^{abc} , which violates C-parity conservation. We are therefore left only with graphs of type (a). These can further be divided into four groups. Each group can be obtained from those shown in Fig. 2 by permutations of the three light quark lines. Since it is usual to treat the heavy $c\bar{c}$ as a non-relativistic system, the heavy quarks share the energy and momentum equally or in other words, the distribution amplitude of the charmonium is taken to be a delta function which peaks at one-half. With this assumption, the hard scattering amplitude T_H can be worked out. For P-wave decays, one has to keep the relative momentum K of the $c\bar{c}$ system and expand the hard part around $K = 0$ since only terms quadratic in K survive the \mathbf{k} integration.

Taking Fig. 2 (a) as an example, with x_i , y_i the momentum fractions and $\mathbf{k}_{\perp i}$, $\mathbf{k}'_{\perp i}$ the internal transverse momenta of the valence quarks in the baryon and antibaryon respectively, the virtualities of the internal lines are

$$\begin{aligned}
\mathcal{G}_1 &= x_1 y_1 (4m_c^2) - (\mathbf{k}_{\perp 1} + \mathbf{k}'_{\perp 1})^2 &= \tilde{\mathcal{G}}_1 - (\mathbf{k}_{\perp 1} + \mathbf{k}'_{\perp 1})^2 \\
\mathcal{G}_2 &= (1 - x_1)(1 - y_1) (4m_c^2) - (\mathbf{k}_{\perp 1} + \mathbf{k}'_{\perp 1})^2 &= \tilde{\mathcal{G}}_2 - (\mathbf{k}_{\perp 1} + \mathbf{k}'_{\perp 1})^2 \\
\mathcal{G}_3 &= x_3 y_3 (4m_c^2) - (\mathbf{k}_{\perp 3} + \mathbf{k}'_{\perp 3})^2 &= \tilde{\mathcal{G}}_3 - (\mathbf{k}_{\perp 3} + \mathbf{k}'_{\perp 3})^2 \\
\mathcal{Q} &= (1 - x_1)y_3 (4m_c^2) - (\mathbf{k}_{\perp 1} - \mathbf{k}'_{\perp 3})^2 &= \tilde{\mathcal{Q}} - (\mathbf{k}_{\perp 1} - \mathbf{k}'_{\perp 3})^2 \\
\mathcal{Q}_c &= 2[x_1(1 - y_1) + y_1(1 - x_1)] m_c^2 + (\mathbf{k}_{\perp 1} + \mathbf{k}'_{\perp 1})^2 &= \tilde{\mathcal{Q}}_c + (\mathbf{k}_{\perp 1} + \mathbf{k}'_{\perp 1})^2
\end{aligned} \tag{27}$$

In fact, Fig. 2 (a) and (b) give identical contributions and the similar contributions from Fig. 2 (c) and (d) can be obtained by interchanging x and y . One gets, after sorting and

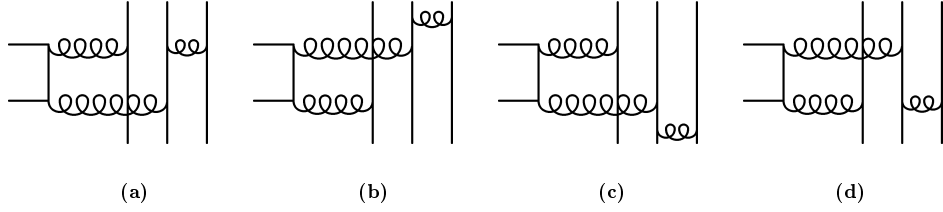


Figure 2: Graphs of type Fig. 1 (a) can be divided further into four groups.

integrating out K , for the hard scattering amplitude

$$\begin{aligned}
T_H^J(x, y, \mathbf{k}_\perp, \mathbf{k}'_\perp) &= \frac{2^{10} \sqrt{2} (4\pi)^3 m_c^5 \alpha_s(t_1) \alpha_s(t_2) \alpha_s(t_3)}{9\sqrt{3} (\mathcal{G}_1 + i\epsilon) (\mathcal{G}_2 + i\epsilon) (\mathcal{G}_3 + i\epsilon) (\mathcal{Q} + i\epsilon) (\mathcal{Q}_c - i\epsilon)} \\
&\times y_3 \left[(1 - 2x_1)^{2-J} + \frac{(-1)^{J-1} 2m_c^2 x_1(x_1 - y_1)}{(\mathcal{Q}_c - i\epsilon)} \right] \\
&+ (x \longleftrightarrow y). \tag{28}
\end{aligned}$$

To improve perturbation theory via renormalization group, the square of the renormalization scale μ_R for each running coupling is set to one of the virtualities $t_i, i = 1, 2, 3$, which are chosen by [12, 13]

$$t_1 = \max(\tilde{\mathcal{G}}_1, \tilde{\mathcal{Q}}_c, 1/b_1^2, 1/b_1'^2) \quad t_2 = \max(\tilde{\mathcal{G}}_2, \tilde{\mathcal{Q}}, 1/b_2^2, 1/b_2'^2) \quad t_3 = \max(\tilde{\mathcal{G}}_3, 1/b_3^2, 1/b_3'^2) \tag{29}$$

with $n_f = 4$ and $\Lambda_{\text{QCD}} = 220$ MeV.

These must be convoluted with the wavefunctions to obtain the colour singlet decay form factors. In transverse separation space and in terms of the expressions,

$$\mathcal{C}_1^J(x, y) = y_3 (1 - 2x_1)^{2-J} \tag{30}$$

$$\mathcal{C}_2^J(x, y) = (-1)^{J-1} y_3 x_1(x_1 - y_1) \tag{31}$$

the hard scattering part \hat{T}_H^J is

$$\begin{aligned}
\hat{T}_H^J(x, y, \mathbf{b}, \mathbf{b}') &= \frac{2^9 \sqrt{2} m_c}{9\sqrt{3}} \alpha_s(t_1) \alpha_s(t_2) \alpha_s(t_3) \delta^2(\mathbf{b}_1 - \mathbf{b}'_1 - \mathbf{b}_3 + \mathbf{b}'_3) \\
&\times \frac{i\pi}{2} H_0^{(1)}(\sqrt{x_3 y_3} (2m_c) |\mathbf{b}_3|) \frac{i\pi}{2} H_0^{(1)}(\sqrt{(1-x_1) y_3} (2m_c) |\mathbf{b}_1 - \mathbf{b}'_1|) \\
&\times \left\{ i\pi \left[\frac{H_0^{(1)}(\sqrt{x_1 y_1} (2m_c) |\mathbf{b}'_1|)}{(x_1 + y + 1)(1 - x_1 - y_1)} \left(\mathcal{C}_1^J(x, y) + \frac{\mathcal{C}_2^J(x, y)}{x_1 + y_1} \right) \right. \right. \\
&\quad \left. \left. - \frac{H_0^{(1)}(\sqrt{(1-x_1)(1-y_1)} (2m_c) |\mathbf{b}'_1|)}{(1-x_1-y_1)(2-x_1-y_1)} \left(\mathcal{C}_1^J(x, y) + \frac{\mathcal{C}_2^J(x, y)}{2-x_1-y_1} \right) \right] \right\}
\end{aligned}$$

$$\begin{aligned}
& \frac{4 K_0^{(1)}(\sqrt{x_1(1-y_1)+y_1(1-x_1)}m_c|\mathbf{b}'_1|)}{\pi (x_1+y_1)(2-x_1-y_1)} \\
& \left(\mathcal{C}_1^J(x,y) + \frac{2 \mathcal{C}_2^J(x,y)}{(x_1+y_1)(2-x_1-y_1)} \right) \\
& \left. \frac{2m_c|\mathbf{b}'_1| \mathcal{C}_2^J(x,y) K_1^{(1)}(\sqrt{x_1(1-y_1)+y_1(1-x_1)}m_c|\mathbf{b}'_1|)}{\sqrt{x_1(1-y_1)+y_1(1-x_1)}(2-x_1-y_1)(x_1+y_1)} \right\} \\
& + \left((x, \mathbf{b}) \longleftrightarrow (y, \mathbf{b}') \right) \quad . \quad (32)
\end{aligned}$$

With this, the decay form factor can be expressed as

$$\begin{aligned}
\mathcal{B}_J^{B(1)} = & -i \frac{\sqrt{3}|R'_p(0)| \sigma_J}{8\sqrt{\pi}m_c^{3/2}} \int [dx][dy] \frac{d^2\mathbf{b}_1}{(4\pi)} \frac{d^2\mathbf{b}_3}{(4\pi)} \frac{d^2\mathbf{b}'_1}{(4\pi)} \frac{d^2\mathbf{b}'_3}{(4\pi)} \hat{T}_H^J(x,y,\mathbf{b},\mathbf{b}') \\
& \exp[-S(x,y,\mathbf{b},\mathbf{b}',2m_c)] \quad \|\hat{\Psi}^B(x,\mathbf{b})\hat{\Psi}^B(y,\mathbf{b}')\| \quad (33)
\end{aligned}$$

where $\sigma_J = 1/\sqrt{2}$, 1 for $J = 1, 2$ respectively, and Sudakov correction factor evaluated at the scale of $2m_c$ is included in the convolution. As mentioned earlier, the presence of this radiative correction in the intermediate scale range, together with the MAX prescription for the infrared cut-off in the Sudakov factor, $\tilde{b} = \max(b_1, b_2, b_3, b'_1, b'_2, b'_3)$, renders the whole approach self-consistent. Actually, since there are two hadrons in the final state, one can have a separate infrared scale for each hadron, for example $\tilde{b} = \max(b_1, b_2, b_3)$ and $\tilde{b}' = \max(b'_1, b'_2, b'_3)$. However, numerically this would make no difference so we merge the two into one scale. The factorization scale μ_F in the wavefunction is then set to $\mu_F = 1/\tilde{b}$ as usual.

The spin structure of the contribution from the diagrams of Fig. 2 requires the J_z of the charmonium to be equal to S_z of the quark line that is not attached to other light quark lines via gluon, i.e. the first quark line from the left of the three vertical lines in any of the figures in Fig. 2. This permits two possibilities for the helicities, that is $(+, +, -)$ and $(+, -, +)$ of the u and d-quark lines in Fig. 2 from left to right. The hard scattering amplitudes are, however, identical for the two arrangements of helicities. This gives the following sums of products of the Fourier transform of the scalar functions Ψ_{123}^B of the baryon-antibaryon, given in Eq. (6) and Eq. (17), represented in Eq. (33) by $\|\hat{\Psi}^B(x,\mathbf{b})\hat{\Psi}^B(y,\mathbf{b}')\|$.

$$\begin{aligned}
\|\hat{\Psi}^{B_8}(x,\mathbf{b})\hat{\Psi}^{B_8}(y,\mathbf{b}')\| = & 2 \left\{ \hat{\Psi}_{123}^{B_8}(x,\mathbf{b})\hat{\Psi}_{123}^{B_8}(y,\mathbf{b}') + \hat{\Psi}_{321}^{B_8}(x,\mathbf{b})\hat{\Psi}_{321}^{B_8}(y,\mathbf{b}') \right. \\
& + \left(\hat{\Psi}_{123}^{B_8}(x,\mathbf{b}) + \hat{\Psi}_{321}^{B_8}(x,\mathbf{b}) \right) \left(\hat{\Psi}_{123}^{B_8}(y,\mathbf{b}') + \hat{\Psi}_{321}^{B_8}(y,\mathbf{b}') \right) \\
& \left. + (2 \longleftrightarrow 3) \right\} \quad (34) \\
\|\hat{\Psi}^\Lambda(x,\mathbf{b})\hat{\Psi}^\Lambda(y,\mathbf{b}')\| = & 6 \left\{ \hat{\Psi}_{123}^\Lambda(x,\mathbf{b})\hat{\Psi}_{123}^\Lambda(y,\mathbf{b}') + \hat{\Psi}_{321}^\Lambda(x,\mathbf{b})\hat{\Psi}_{321}^\Lambda(y,\mathbf{b}') \right.
\end{aligned}$$

J	$\Gamma^{(1)}(\chi_J \rightarrow p\bar{p})$ (eV)	PDG (eV) [23]	BES (eV) [29]
1	2.53	75.68	37.84
2	16.58	200.00	118.00

Table 2: Clearly, the colour singlet contributions are insufficient in explaining the experimental data of χ_J decay into $p\bar{p}$.

$$\begin{aligned}
& + \left(\hat{\Psi}_{123}^{\Lambda}(x, \mathbf{b}) - \hat{\Psi}_{321}^{\Lambda}(x, \mathbf{b}) \right) \left(\hat{\Psi}_{123}^{\Lambda}(y, \mathbf{b}') - \hat{\Psi}_{321}^{\Lambda}(y, \mathbf{b}') \right) \\
& + (2 \longleftrightarrow 3) \} \tag{35}
\end{aligned}$$

$$\begin{aligned}
\| \hat{\Psi}^{B_{10}}(x, \mathbf{b}) \hat{\Psi}^{B_{10}}(y, \mathbf{b}') \| = 3 \left\{ \hat{\Psi}_{123}^{B_{10}}(x, \mathbf{b}) \hat{\Psi}_{123}^{B_{10}}(y, \mathbf{b}') + \hat{\Psi}_{321}^{B_{10}}(x, \mathbf{b}) \hat{\Psi}_{321}^{B_{10}}(y, \mathbf{b}') \right. \\
\left. + \hat{\Psi}_{132}^{B_{10}}(x, \mathbf{b}) \hat{\Psi}_{132}^{B_{10}}(y, \mathbf{b}') + \hat{\Psi}_{231}^{B_{10}}(x, \mathbf{b}) \hat{\Psi}_{231}^{B_{10}}(y, \mathbf{b}') \right\} \tag{36}
\end{aligned}$$

The results for the colour singlet contributions in χ_1 and χ_2 decay into nucleon-antinucleon are shown in Table 2³ together with the experimental measurements. It is clear that the singlet contribution is insufficient even with the smaller results of the BES collaboration [29] to account for the experimental measurements. For uncertainties in the theoretical estimate of the colour singlet contribution, the consistency of this calculation within MHSa, the choice of proton wavefunction and the value of the proton decay constant used etc., we refer to [14]. We will discuss more about the differences between the experimental results in later section. The very important colour octet contribution will be investigated in the following section.

7 Colour Octet Contribution

In colour octet $c\bar{c}$ decays into baryon-antibaryon, there is a constituent gluon in the initial state so the C-parity arguments given in Sec. 6 no longer hold. The diagrams in Fig. 1 then form the bases of three different contributing groups. The other possibilities are from the graphs where the $c\bar{c}$ pair annihilates into a single gluon which would not be possible, if the pair were in a colour singlet state. These additional groups are shown in Fig. 3.

In order to form colour singlet baryon-antibaryon in the final states, this net colour from the constituent gluon must be neutralized. One could allow it to enter directly into one of the final baryons as a constituent of a higher Fock state of the latter. However, within the hard scattering approach, at least one hard gluon must be exchanged between all the constituent partons, therefore such contribution involving the next higher Fock state of the baryons will be suppressed by the hard scale of the process and also by

³Our present numbers supersede those previously reported in [30].

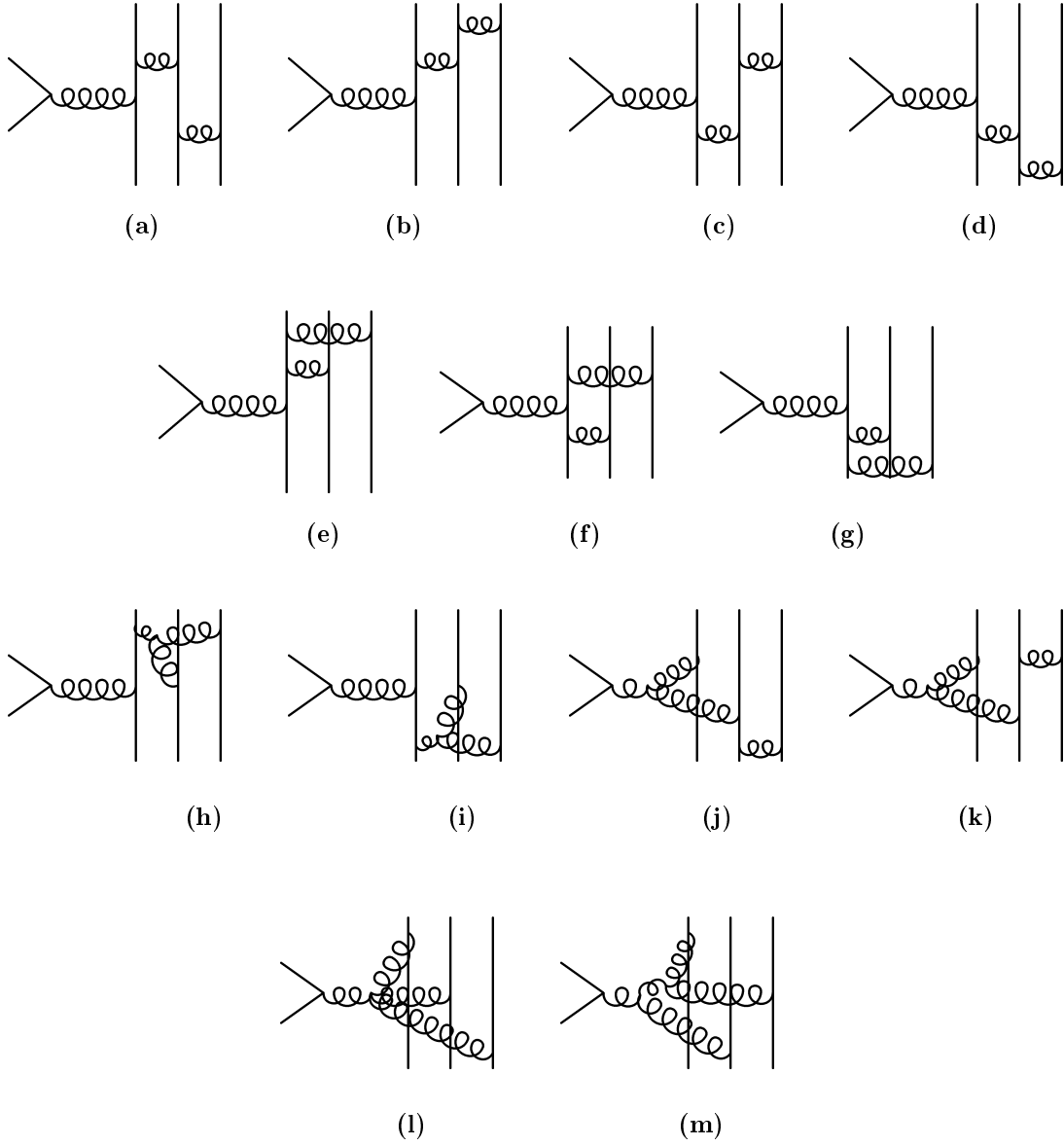


Figure 3: In addition to the graphs of type Fig. 1, these form the bases of further contributions in the colour octet decay channel.

the smaller probability of the next Fock state. In any case, bringing in a higher state unnecessarily will introduce additional unknown wavefunctions. It is therefore best to avoid it. The introduction of the colour octet in the charmonium system is, on the contrary, well founded and is indeed necessary as shown in [3, 4] and as we argued earlier. The alternative for colour neutralization is done by attaching the constituent gluon onto all possible places in the diagrams of Fig. 1, Fig. 2 and Fig. 3. This will generate about 9–11 diagrams for each group and the light quark lines will also have to be permuted and so altogether there are over two hundred diagrams. Fortunately, the tedious algebra can be handled completely by the computer program FORM, and one can arrange the constituent gluon to be attached automatically to all possible places in each basic graph and worked out the colour factors as well as the perturbative hard scattering part entirely by using this program. In fact, none of the algebra needs to be worked out by hand.

The colour octet wavefunction of the charmonium is

$$|\chi_{\chi_J}^{(8)}, p\rangle = \frac{t_{c\bar{c}}^a}{2} f_{\chi_J}^{(8)} \int [dz] \phi_{\chi_J}^{(8)}(z_1, z_2, z_3) S_{J\nu}^{(8)}(p) |c\bar{c}g; p\rangle. \quad (37)$$

As explained in [11], the distribution amplitude of the octet charmonium $\phi_{\chi_J}^{(8)}$ is conveniently taken to be delta functions that peak at the light-cone momentum $z_3 = z = 0.15$ for the constituent gluon and $z_1 = z_2 = (1 - z)/2$ for the heavy quarks while the octet decay constant $f_{\chi_J}^{(8)}$ are obtained from fits in [20, 21]. The covariant spin wavefunctions for the octet states are given in [21]

$$\begin{aligned} S_{1\rho}^{(8)}(p) &= \frac{-i}{2M_{\chi_1}} (\not{p} + M_{\chi_1}) \epsilon_{\mu\nu\rho\sigma} \not{p}^\mu \epsilon^\nu \gamma^\sigma \\ S_{2\rho}^{(8)}(p) &= \frac{1}{\sqrt{2}} (\not{p} + M_{\chi_2}) \epsilon_{\sigma\rho} \gamma^\sigma. \end{aligned} \quad (38)$$

As we will take the spin of the charmonium to be pointing upward without loss of generality, we found it more straight forward to write these as

$$S_{1\rho}^{(8)(+)}(p) = \frac{1}{2} (\not{p} + M_{\chi_1}) (\not{\epsilon}_{c\bar{c}}^{(+)} \epsilon_\rho^{(0)} - \not{\epsilon}_{c\bar{c}}^{(0)} \epsilon_\rho^{(+)}) \quad (39)$$

$$S_{2\rho}^{(8)(+)}(p) = \frac{1}{2} (\not{p} + M_{\chi_2}) (\not{\epsilon}_{c\bar{c}}^{(+)} \epsilon_\rho^{(0)} + \not{\epsilon}_{c\bar{c}}^{(0)} \epsilon_\rho^{(+)}) \quad (40)$$

instead. The ϵ_ρ is the polarization vector of the constituent gluon and $\epsilon_{c\bar{c}}^\mu$ is the spin S=1 vector of the colour octet $c\bar{c}$ system. Then the numerator of any contributing graphs to χ_J decay can all be expressed in the form of

$$N^J = \mathcal{A} + (-1)^J \mathcal{A}' \quad (41)$$

and the difference in the numerator between the χ_1 and χ_2 system comes entirely from the sign. In the appendix where we list all the contributions from the graphs of each group, the numerators are all in the above format.

To deal with the colour octet contributions, bearing in mind that the advantages of the dynamical setting of the renormalization scales and the built-in Sudakov suppression of the end-point problematic regions of the distribution amplitudes, one could use again the modified hard scattering scheme [12, 13] as we did in the singlet contribution in the previous section. However, these advantages are obtained at the expense of complicating the expressions and the calculations of the perturbative hard part $T_H(x, \mathbf{k}_\perp)$ by including the internal transverse momenta in the propagators. These transverse momenta will have to be integrated out subsequently by convoluting with the hadronic wavefunctions. Therefore the number of integration variables can be quite high especially when we are dealing with baryon and antibaryon which contain three constituent quarks and antiquarks even at the valence level and also there are many diagrams to consider. To keep things simple, it is advisable to return to the standard scheme [1] so as to deal only with distribution amplitudes and $T_H(x)$ without the internal transverse momenta and not the more complicated wavefunctions and $T_H(x, \mathbf{k}_\perp)$. This is what we will do below. We will discuss getting the graphs and the expressions for the individual colour octet contribution to the amplitude in the next section within the standard scheme.

8 Getting The Graphs And Calculating T_H Of The Colour Octet Contributions

In the appendices, we give the graphs and expressions of our calculation for the colour octet contribution. The diagrams can be divided into ten basic groups. Each group is based on one basic graph in which the constituent gluon from the colour octet component of the charmonium has not yet been drawn or inserted. Because of the restriction of C-parity, in the absence of the constituent gluon, these groups individually may or may not exist in the colour singlet contribution to the decay. In the latter case, they survive solely because of the presence of the constituent gluon. These graphs are those already presented in Fig. 1 and Fig. 3. The group associated with each basic graph is generated by attaching the constituent gluon to all possible places on the basic graph except on the initial c -quark or \bar{c} -quark when they have just emerged from the charmonium.

The numerator of the hard part T_H of each diagram from each group will be given in the appendices, while the denominator which is essentially a product of the propagators in each diagram, will not be written out explicitly individually but can be derived from those of the basic graphs (these will be presented with each group) by following some simple rules that followed from the momentum flow through the graph. Given that the momenta of the χ_J , and those of the outgoing baryon and antibaryon are P_{χ_J} , P_B and $P_{\bar{B}}$ respectively, the outgoing momenta of the constituents of the baryon and antibaryon will be assigned the momenta $p_{q_i} = x_i P_B$, $p_{\bar{q}_i} = y_i P_{\bar{B}}$ with $i = 1, 2, 3$. Here x_i and y_i are the momentum fraction of the i light quark line of the outgoing baryon-antibaryon subjected to $\sum_i x_i = \sum_i y_i = 1$. In the basic graphs, the constituent gluon is not included

so the momentum of χ_J shared by the charm-anticharm is $p_c = z_1 P_{\chi_J}$ and $p_{\bar{c}} = z_2 P_{\chi_J}$ with $z_1 + z_2 = 1$. Obviously energy-momentum conservation requires $P_{\chi_J} = P_B + P_{\bar{B}}$. The product of the gluon propagators in each of the basic graphs is expressed with these momentum configurations with $2P_B \cdot P_{\bar{B}} = (2m_c)^2 \gg P_B^2, P_{\bar{B}}^2 \sim 0$. On the insertion of the constituent gluon with momentum fraction z , the condition $z_1 + z_2 = 1$ is now replaced by $z + z_1 + z_2 = 1$. Therefore the heavy quark pair will have only $(1 - z)P_{\chi_J}$ instead of the full P_{χ_J} to annihilate into gluons. The consequence is that in the new graphs the momenta flowing along the path or lines connecting the initial heavy quark line of the charmonium to the insertion point of the constituent gluon must be reduced by zP_{χ_J} . The momenta in any intermediate heavy quark line(s) which only exist in those graphs where the $c\bar{c}$ annihilates into two or more gluons, may also need to be so-adjusted but that depends on the insertion point. This momentum shift in the basic graphs brings about a similar shift in the momenta carried by the propagators along the same connecting path. In general, this shift can be done by replacing one of the three (x_i, y_i) pairs in the affected propagators including the intermediate heavy quark one by $(x_i - z, y_i - z)$.

The momentum fractions and the quark and gluon lines are labelled as follows for simpler description and they apply to all basic graphs. The top (bottom) heavy quark line on the left is the initial charm (anticharm) quark line. The three vertical light quark lines running from the bottom to the top are light quark line 1 to 3 from left to right. Light quarks (antiquark) of the baryon (antibaryon) emerge from the top (bottom). The fraction x_i and y_i label that of the quark and antiquark of the i light quark line. The gluon line coming directly or indirectly from the charmonium and entering the i light quark line is gluon line i , G_i . Whereas the labelling of the vertical light quark line is for the entire line, each of these gluon lines connects only two vertices and ends at these vertices. There will be only one gluon line entering each light quark line even though each light quark line may be attached to more than one gluon line. In this case, only one such line enters the quark line and the other is leaving it. The gluon line is then labelled with G_i if it is entering light quark line i and not leaving it as we mentioned above. Fig. 4 illustrates our labelling scheme with some examples. There are however gluon lines that enter a 3- or 4-gluon vertex instead of a light quark line, see Group 4 and 6 for example. These are not labelled. The labelling is for the purpose of identifying the graphs created from the basic one by the insertion of the constituent gluon. The insertion point (I.P.) of the constituent gluon will uniquely identify each so-created graph and these graphs will form a group based on the basic one. Taking the χ_1 and χ_2 to be spinning up. The allowed helicities of the three light quark lines $(\lambda_1, \lambda_2, \lambda_3)$ are $(+, +, -)$, $(+, -, +)$ and $(-, +, +)$. These three helicities configurations of each graph do not necessarily have the same or permutation related numerator as in the colour singlet case. The presence of the constituent gluon makes this not possible in general. The corresponding numerators are listed in the tables in the appendices.

As mentioned above, each graph created from a basic graph by adding the constituent gluon is identified by the insertion point where the gluon from the colour octet state of

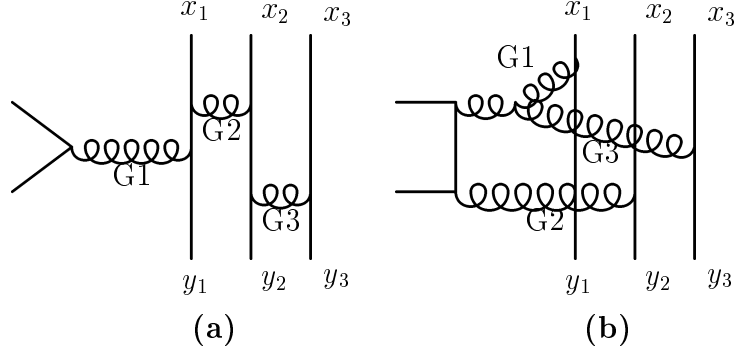


Figure 4: Our labelling scheme as applied to (a) Group 2 and (b) Group 4.

the charmonium joins the basic graph. The group of a basic graph is created by attaching the colour octet gluon to all possible places on the basic graph with the exception of the initial heavy quark or antiquark line. Also the creation of a graph with an intermediate state with one gluon and nothing else is forbidden by C-parity. More explicitly it means that when the basic graph contains the $c\bar{c}$ annihilation into one single gluon, the graph with the constituent gluon attached to this gluon is not possible. Note that this kind of basic graphs by themselves cannot exist without the constituent gluon because of C-parity and so they do not contribute to the colour singlet contribution.

The complete graphs created from the basic ones will be labelled as follows. If the constituent gluon attaches to one of the light quark lines, it can be with one of the three quarks (antiquarks) that forms the baryon (antibaryon). These graphs are labelled as U_i or L_i indicating that the constituent gluon joins the upper (top) or lower (bottom) part of the quark line i . If the quark line has one or more intermediate off-shell middle segment, which is or are separated from the upper and lower part by quark-gluon-antiquark vertex or vertices, to which the octet gluon attaches itself, these are labelled M_i for one intermediate off-shell quark line on quark line i , for example the quark line 2 of Group 1 (see Fig. 7), and UM_i or LM_i denoting upper or lower part of the middle off-shell line if two intermediate middle segments exist on the light quark line i , for example the quark line 1 of Group 8 (see Fig. 15). Evidently, the constituent gluon can be attached to the gluon lines as well. These graphs are labelled with G_i (not to be confused with the gluon line labelling) if the new graph is created by joining the gluon to the gluon line i by a 3-gluon vertex. If the gluon is attached instead to an unlabelled gluon line, the graph will be called GR as the constituent gluon attaches to the remaining unlabelled gluon line. Only one such graph per group is possible at maximum and these always vanish due to colour. We will not discuss these graphs further. Whenever a 3-gluon vertex exists in a basic graph, there is the possibility of attaching the constituent gluon to this vertex to create a complete graph with a 4-gluon vertex. These will be labelled as 4G for one such possibility or 4G1 and 4G2 when two such possibilities exist as in Group 9 (see Fig. 16). There remains attaching the gluon to the heavy intermediate heavy quark line(s) when

this exists. We denote this simply by graph Q for only one heavy quark line or UQ and LQ in the presence of two heavy quark lines, one situated above the other on the basic graph, meaning the gluon is attached to the upper or lower heavy quark line. This latter is possible only for Group 5.

The rules for getting the product of propagators for each new graph from that of the basic graphs are as follows. In determining which of the pair (x_i, y_i) in the propagators to replace by $(x_i - z, y_i - z)$, it is the i pair for graphs labelled U_i, L_i, G_i, M_i, UMi or LMi . The replacement should only be made to propagators along the line connecting the heavy quark line to the insertion point whether they contain (x_i, y_i) explicitly or not. Modification must be made to gluon or light quark propagators through the relation $x_i = 1 - x_j - x_k$ and $y_i = 1 - y_j - y_k$ where $j \neq k \neq i$ and also to any charm propagator only if it contains the pair (x_i, y_i) explicitly. So applying this to graph U1 of Group 5 illustrated in Fig. 5(a), only the propagators associated with the gluon line G1 and the upper heavy quark line in Fig. 12 need this replacement. The product becomes

$$\frac{1}{\{(z_1+z-x_1)(z_1+z-y_1)-1/4\}(2m_c)^2} \frac{1}{\{(z_2-x_3)(z_2-y_3)-1/4\}(2m_c)^2} \frac{1}{(x_1-z)(y_1-z)(2m_c)^2+\rho^2} \frac{1}{x_2y_2(2m_c)^2} \frac{1}{x_3y_3(2m_c)^2} \cdot \quad (42)$$

If it is graph L2 of Group 5 in Fig. 5(b), only the propagator of gluon line G2 needs to be changed and we have

$$\frac{1}{\{(z_1-x_1)(z_1-y_1)-1/4\}(2m_c)^2} \frac{1}{\{(z_2-x_3)(z_2-y_3)-1/4\}(2m_c)^2} \frac{1}{x_1y_1(2m_c)^2} \frac{1}{(x_2-z)(y_2-z)(2m_c)^2+\rho^2} \frac{1}{x_3y_3(2m_c)^2} \cdot \quad (43)$$

As a third example, applying this to Fig. 5(c) that is graph L3 of Group 1 gives

$$\frac{1}{(1-z)^2(2m_c)^2} \frac{1}{(x_3-z)(1-y_1-z)(2m_c)^2+\rho^2} \frac{1}{x_1y_1(2m_c)^2} \frac{1}{(1-x_1-z)(1-y_1-z)(2m_c)^2+\rho^2} \frac{1}{(x_3-z)(y_3-z)(2m_c)^2+\rho^2} \cdot \quad (44)$$

It must be mentioned that in the appendices where details of each group are given, the propagators are written down without the usual $i\epsilon$. This is to save on typing but it should be understood implicitly that a $i\epsilon$ should be present in each propagator. This also applies to the expressions here. Also, we have inserted a term ρ^2 in the denominators of those propagators which carry two poles which cannot be handled by the $i\epsilon$ prescription. The ρ^2 is understood to be the mean-squared internal momentum of the baryons $\rho^2 = \langle \mathbf{k}_\perp^2 \rangle$. It is used here to prevent two possible poles in any one propagator to occur simultaneously. This problem has been treated in the same manner in [20] whenever the $i\epsilon$ prescription failed. The actual values of ρ^2 depend on the baryon wavefunctions. We used $\rho_{(8)} = 415.0$ MeV and $\rho_{(10)} = 389.0$ MeV for the octet and decuplet baryons, respectively. These values are obtained from the respective wavefunctions.

For 4G graphs, if the unlabelled gluon line attaches to the 3-gluon vertex connecting gluon line G_i and G_j , then either replace (x_i, y_i) with $(x_i - z, y_i - z)$ or (x_j, y_j) with

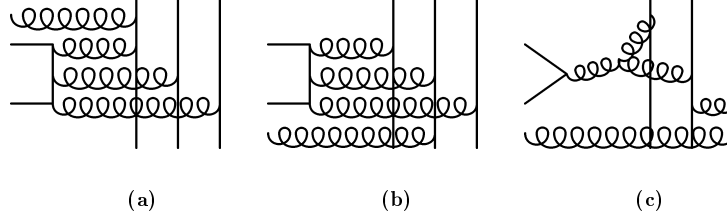


Figure 5: Examples of complete colour octet graphs. (a) graph U1 and (b) graph L2 of Group 5, and (c) graph L3 of Group 1.

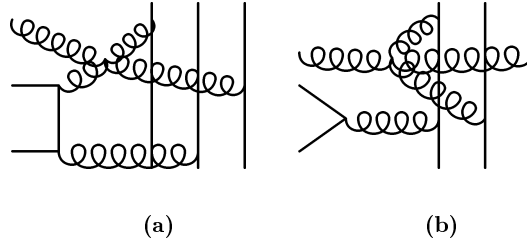


Figure 6: Examples of complete colour octet graphs with 4-gluon vertex. (a) graph 4G of Group 4 and (b) graph 4G of Group 10.

$(x_j - z, y_j - z)$ in the gluon propagator and do the same in the heavy quark propagator but in this case only when either pair of momentum fractions appears explicitly is sufficient. Applying this to Group 4, we get

$$\frac{1}{\{(z_2 - x_2)(z_2 - y_2) - 1/4\}(2m_c)^2} \frac{1}{(1 - x_2 - z)(1 - y_2 - z)(2m_c)^2 + \rho^2} \frac{1}{x_1 y_1 (2m_c)^2} \frac{1}{x_2 y_2 (2m_c)^2} \frac{1}{x_3 y_3 (2m_c)^2} , \quad (45)$$

and to Group 10, the product of propagator become

$$\frac{1}{(1 - z)^2 (2m_c)^2} \frac{1}{(1 - z)(1 - y_1 - z)(2m_c)^2} \frac{1}{(1 - x_1 - z)(1 - y_1 - z)(2m_c)^2 + \rho^2} \frac{1}{x_2 y_2 (2m_c)^2} \frac{1}{x_3 y_3 (2m_c)^2} . \quad (46)$$

Eq. (44) and Eq. (46) are fine examples of the necessity of having to make the shift even if either pair of momentum fractions does not appear explicitly in the light quark and gluon propagators. In these example, the replacement has to be made even for $x_1 + x_2 + x_3 = y_1 + y_2 + y_3 = 1$ to $1 - z$ because the momentum fractions are completely hidden. For the remaining Q, UQ and LQ graphs, it is only necessary to replace z_1 by $z_1 + z$ and z_2 must be left alone.

One must not forget that the insertion of the constituent gluon will introduce an additional propagator (X-Prop.) to the basic graph. This is, however, not true for the

4G graphs but these have a factor $(2m_c)^2$ less than the other graphs and so a factor of $1/(2m_c)^2$ must be multiplied to them so that a global prefactor can be written down for all graphs. The extra propagator or the extra factor $1/(2m_c)^2$ is given in the last table of numerators of each group under the column X-Prop. Similarly, the structure of group 6 is such that it is a factor $(2m_c)^2$ less than the other group from the start because these graphs have one less propagator. In order to keep the same overall factor for all groups, $1/(2m_c)^2$ has been multiplied to the product of the basic propagators of this group. This extra factor of course does not correspond to any propagator but is merely a compensation factor. It must be mentioned that not all graphs generated from the basic graphs exist. Some vanish for one reason or another. For these, the additional propagators are not given in the tables but have the entry n. g. (not given) instead.

There exist several more groups that we have not drawn out explicitly in the appendices. Their basic graphs may be obtained from those of Group 1, 2 and 2', 3, 4, 7 and 10 by making one simple change to them. For example, attaching the line G2 to quark line 1 at a point below instead of above the line G1 on Group 2 and 2', or moving line G3 in Group 1 and 3 to above the $qg\bar{q}$ -vertex on quark line 2, or flipping any of the basic graphs of Group 3, 4, 7 and 10 upside down. However, these extra groups may be included by giving a factor of two on each of their associated group because these are related to each other by a simple change of variables. Finally, we must mentioned that the graphs in each group must be subjected to further permutations of the three light quark lines to give further graphs. But these also can be taken care of by a numerical factor so each possible insertion point will generate only one graph and there is no need to divide the graphs any further or add any more groups.

9 Colour Singlet And Octet Contribution In The Standard Scheme

9.1 Colour Singlet Contribution

The procedure to obtain the colour singlet contribution in the standard scheme is quite similar to the one we used in Sec. 6. Remembering that in the standard scheme, the internal transverse momenta are taken to be negligible in comparison with the virtualities in all propagators in the perturbative hard part, so $T_H(x)$ is free from any \mathbf{k}_\perp 's and the latter can be integrated over each wavefunction to give the corresponding distribution amplitude. So setting the \mathbf{k}_\perp 's in \mathcal{G}_i , \mathcal{Q} and \mathcal{Q}_c in Eq. (27) to zero, T_H^J is now independent of \mathbf{k}_\perp and \mathbf{k}_\perp'

$$T_H^J(x, y) = \frac{2\sqrt{2} (4\pi)^3 (\alpha_s(m_c))^3}{9\sqrt{3}m_c^5 x_1x_3y_1y_3 (1-x_1)^2(1-y_1) [x_1(1-y_1) + y_1(1-x_1)]}$$

$$\begin{aligned}
& \times \left[(1 - 2x_1)^{2-J} + \frac{(-1)^{J-1} x_1(x_1 - y_1)}{x_1(1 - y_1) + y_1(1 - x_1)} \right] \\
& + (x \longleftrightarrow y) .
\end{aligned} \tag{47}$$

The renormalization scale μ_R in the above equation has been set at the constant scale m_c in α_s because each gluon takes approximately $M_{\chi_J}/2 \approx m_c$ from the charmonium and so the virtuality is roughly m_c^2 . Now Fourier transforming the transverse momentum independent T_H^J to transverse position-space yields several delta functions which force all \mathbf{b} 's and \mathbf{b}' 's to the origin. As a consequence, following from its definition and derivation, the Sudakov factor has to be set to unity. The decay form factor defined in Sec. 5 of χ_J into $B - \bar{B}$ becomes

$$\mathcal{B}_J^{B(1)} = -i \frac{\sqrt{3} |R'_p(0)| \sigma_J}{8\sqrt{\pi} m_c^{3/2} (4\pi)^4} \int [dx][dy] T_H^{J(1)}(x, y) \|\hat{\Psi}^B(x, 0)\hat{\Psi}^B(y, 0)\| \tag{48}$$

where $\sigma_J = 1/\sqrt{2}, 1$ for $J = 1, 2$ as before. This has to be combined with that of the colour octet contribution to be discussed below in accordance with our theoretical arguments given in Sec. 3 to give the true partial decay width.

9.2 Colour Octet Contribution

The total colour octet contribution to $\mathcal{B}_J^{B(8)}$ has to be the sum over all contributing graphs from each group and over all possible helicity configurations of the light quarks and antiquarks in the outgoing baryon-antibaryon given in the appendices

$$\mathcal{B}_J^{B(8)} = \sum_{\lambda_1, \lambda_2, \lambda_3 = \pm} \frac{f_{\chi_J}^{(8)} \sigma_J}{2m_c (4\pi)^4} \int [dx][dy] \{T_H^{J(8)}(x, y)\}_{\lambda_1, \lambda_2, \lambda_3} \|\hat{\Psi}^B(x, 0)\hat{\Psi}^B(y, 0)\|_{\lambda_1, \lambda_2, \lambda_3} . \tag{49}$$

The helicity dependent hard perturbative parts are

$$\begin{aligned}
\{T_H^{J(8)}(x, y)\}_{\lambda_1, \lambda_2, \lambda_3} &= i (4\pi\alpha_s(m_c))^3 \sqrt{4\pi\alpha_s^{soft}} (2m_c)^7 \\
&\times \sum_{\substack{g \in \text{Groups} \\ m \in \text{Members}}} S_g P_{gm}(x, y) \{N_{gm}^J(x, y)\}_{\lambda_1, \lambda_2, \lambda_3}
\end{aligned} \tag{50}$$

where $P_{gm}(x, y)$ is the product of propagators of the member $m = \text{U1, U2, U3, L1, L2, L3, } \dots$ etc. of the group $g = 1, 2, 2', \dots, 10$. They can be obtained from the product of the basic propagators of each group as discussed in Sec. 8. The S_g is a symmetry factor for the group g to take care of similar potential groups that are related to g by simple change of variables. For the groups listed in the appendices, $S_g = \{2, 2, 2, 4, 2, 1, 1, 2, 1, 1, 2\}$ for the

group $g = 1, 2, 2', 3, \dots, 10$, respectively. The coupling α_s^{soft} , taken to be equal to π , is that of attaching the constituent gluon to the basic graphs. It needs special treatment because of its different nature in comparison to the rest of the α_s 's [21]. The $\{N_{gm}(x, y)\}_{\lambda_1, \lambda_2, \lambda_3}$ in the above equation contains the helicity dependence and denotes the numerator of the member m of the group g . These numerators are given in the appendices. Note that the calculation is really only gauge-invariant to order z^2 in the numerator (see ref. [21]) because the $c\bar{c}$ are treated as on-shell, therefore all z^3 or higher terms in the numerator have to be dropped. The remaining helicity dependent product of the scalar functions $\Psi_{123}^B(x, 0)$ of the baryon wavefunctions are given below.

$$\begin{aligned} \|\hat{\Psi}^{B_8}(x, 0)\hat{\Psi}^{B_8}(y, 0)\|_{+,+,-} &= 2 \left\{ \hat{\Psi}_{132}^{B_8}(x, 0)\hat{\Psi}_{132}^{B_8}(y, 0) + \hat{\Psi}_{231}^{B_8}(x, 0)\hat{\Psi}_{231}^{B_8}(y, 0) \right. \\ &\quad \left. + \left(\hat{\Psi}_{132}^{B_8}(x, 0) + \hat{\Psi}_{231}^{B_8}(x, 0) \right) \left(\hat{\Psi}_{132}^{B_8}(y, 0) + \hat{\Psi}_{231}^{B_8}(y, 0) \right) \right\} \end{aligned} \quad (51)$$

$$\begin{aligned} \|\hat{\Psi}^{B_8}(x, 0)\hat{\Psi}^{B_8}(y, 0)\|_{+,-,+} &= 2 \left\{ \hat{\Psi}_{123}^{B_8}(x, 0)\hat{\Psi}_{123}^{B_8}(y, 0) + \hat{\Psi}_{321}^{B_8}(x, 0)\hat{\Psi}_{321}^{B_8}(y, 0) \right. \\ &\quad \left. + \left(\hat{\Psi}_{123}^{B_8}(x, 0) + \hat{\Psi}_{321}^{B_8}(x, 0) \right) \left(\hat{\Psi}_{123}^{B_8}(y, 0) + \hat{\Psi}_{321}^{B_8}(y, 0) \right) \right\} \end{aligned} \quad (52)$$

$$\begin{aligned} \|\hat{\Psi}^{B_8}(x, 0)\hat{\Psi}^{B_8}(y, 0)\|_{-,+,+} &= 2 \left\{ \hat{\Psi}_{213}^{B_8}(x, 0)\hat{\Psi}_{213}^{B_8}(y, 0) + \hat{\Psi}_{312}^{B_8}(x, 0)\hat{\Psi}_{312}^{B_8}(y, 0) \right. \\ &\quad \left. + \left(\hat{\Psi}_{213}^{B_8}(x, 0) + \hat{\Psi}_{312}^{B_8}(x, 0) \right) \left(\hat{\Psi}_{213}^{B_8}(y, 0) + \hat{\Psi}_{312}^{B_8}(y, 0) \right) \right\} \end{aligned} \quad (53)$$

$$\begin{aligned} \|\hat{\Psi}^\Lambda(x, 0)\hat{\Psi}^\Lambda(y, 0)\|_{+,+,-} &= 6 \left\{ \hat{\Psi}_{132}^\Lambda(x, 0)\hat{\Psi}_{132}^\Lambda(y, 0) + \hat{\Psi}_{231}^\Lambda(x, 0)\hat{\Psi}_{231}^\Lambda(y, 0) \right. \\ &\quad \left. + \left(\hat{\Psi}_{132}^\Lambda(x, 0) - \hat{\Psi}_{231}^\Lambda(x, 0) \right) \left(\hat{\Psi}_{132}^\Lambda(y, 0) - \hat{\Psi}_{231}^\Lambda(y, 0) \right) \right\} \end{aligned} \quad (54)$$

The other two helicity arrangements of this quantity for the Λ follow the pattern above for the other octet baryons. For the decuplet baryons, they are

$$\begin{aligned} \|\hat{\Psi}^{B_{10}}(x, 0)\hat{\Psi}^{B_{10}}(y, 0)\|_{+,+,-} &= 3 \left\{ \hat{\Psi}_{132}^{B_{10}}(x, 0)\hat{\Psi}_{132}^{B_{10}}(y, 0) + \hat{\Psi}_{231}^{B_{10}}(x, 0)\hat{\Psi}_{231}^{B_{10}}(y, 0) \right\} \\ \|\hat{\Psi}^{B_{10}}(x, 0)\hat{\Psi}^{B_{10}}(y, 0)\|_{+,-,+} &= 3 \left\{ \hat{\Psi}_{123}^{B_{10}}(x, 0)\hat{\Psi}_{123}^{B_{10}}(y, 0) + \hat{\Psi}_{321}^{B_{10}}(x, 0)\hat{\Psi}_{321}^{B_{10}}(y, 0) \right\} \\ \|\hat{\Psi}^{B_{10}}(x, 0)\hat{\Psi}^{B_{10}}(y, 0)\|_{-,+,+} &= 3 \left\{ \hat{\Psi}_{213}^{B_{10}}(x, 0)\hat{\Psi}_{213}^{B_{10}}(y, 0) + \hat{\Psi}_{312}^{B_{10}}(x, 0)\hat{\Psi}_{312}^{B_{10}}(y, 0) \right\}. \end{aligned} \quad (55)$$

With these notations, the colour octet contribution looks rather simple. One only has to sum up all graphs from each and every group and then perform the integrations.

10 The Widths Of χ_J Decay Into Baryons-Antibaryons

With our method discussed in the previous sections, colour octet contribution which we argued to be necessary in addition to the singlet contribution to getting the correct P-wave χ_J partial decay widths can be included. Before giving the numerical results, it must be mentioned that of all the baryons we considered, only the decay into proton-antiproton is measured so the majority of our results are in fact predictions. Moreover, the most recently reported measured values [29] differ by as much as a factor of two from those in the Particle Data Tables [23]. This is also true in the case of the decay into pseudoscalar mesons as noted already in [21]. Therefore we are content with results that lie somewhere in between these measurements. Until the situation improves, the colour octet decay constants fitted in [20, 21] cannot be more accurately determined hence also the current results. In any case, part of our goal is to show that explicit calculations do indeed support the theoretical arguments, that is the colour octet contribution in P-wave χ_J decays cannot be neglected both in inclusive as well as in exclusive process.

Our results are shown in Table 3 for octet and decuplet baryons. The numerical parameters used to obtain these results which were given throughout this paper have been collected together again in appendix B so that any interested readers do not have to search through the paper for their values. Only the kinematically plausible decuplet baryons with the lowest masses are considered. In getting this results, we used the colour octet decay constant $f_{\chi_2}^{(8)} = 0.9 \times 10^{-3} \text{ GeV}^2$ fitted in [20] for the decay of $\chi_2 \rightarrow \pi\pi$ within the standard hard scattering approach. We found that in order to obtain reasonable agreement of the $\chi_1 \rightarrow p\bar{p}$ decay, it must have a smaller colour octet decay constant. Therefore we use $f_{\chi_1}^{(8)} = 0.225 \times 10^{-3} \text{ GeV}^2$. Note that this does not contradict the result in [20], since χ_1 cannot decay into $\pi\pi$ because of parity. and the decay constant $f_{\chi_1}^{(8)}$ is therefore unconstrained in [20]. The smaller colour octet decay constant for the χ_1 than those of the $J = 0, 2$ partners is not too surprising given that the odd-spin P-wave charmonium is a somewhat different heavy quark-antiquark system. Table 3 shows that the decay widths decrease roughly with increasing value of the baryon masses or with the reduction in the available phase space.

In Table 4, the branching ratios of the decays into $p\bar{p}$ is shown against the experimental measurements. As mentioned above, the disagreement between PDG and BES is sizable. This is true not only in the ratios into $p\bar{p}$ but also in the case of a pair of pseudoscalars in the final state. Since our results are based on fit to the latters, until the experimental situation improves, we have to settle for our current results.

From Sec. 6 and Table 4, it is clear that only by including colour octet can the decay

Octet Baryons	$\Gamma^{(1)+(8)}$ (eV)		Decuplet Baryons	$\Gamma^{(1)+(8)}$ (eV)	
	J=1	J=2		J=1	J=2
$\chi_J \rightarrow N\bar{N}$	(56.27)	154.19	$\chi_J \rightarrow \Delta\bar{\Delta}$	33.49	124.62
$\chi_J \rightarrow \Sigma\bar{\Sigma}$	28.42	97.69	$\chi_J \rightarrow \Sigma^*\bar{\Sigma}^*$	18.46	71.09
$\chi_J \rightarrow \Xi\bar{\Xi}$	21.49	72.62	$\chi_J \rightarrow \Xi^*\bar{\Xi}^*$	9.42	41.16
$\chi_J \rightarrow \Lambda\bar{\Lambda}$	33.64	69.19			

Table 3: The partial decay widths for χ_J decay into octet and decuplet baryon-antibaryon pairs. The width of $\chi_1 \rightarrow N\bar{N}$ in parenthesis is to indicate that this value is a fit unlike all partial widths of χ_2 which are predictions. Based on this fit, the rest of χ_1 widths are also predictions.

	Branching ratios ($\times 10^{-5}$)		
	$\text{Br}^{(1)+(8)}$	PDG	BES
$\chi_1 \rightarrow p\bar{p}$	(6.39)	8.60 ± 1.2	$4.30 \pm 2.3 \pm 2.9$
$\chi_2 \rightarrow p\bar{p}$	7.71	10.00 ± 1.0	$5.90 \pm 3.1 \pm 3.3$

Table 4: Comparing our results with the measured widths from the PDG [23] data and from the BES collaboration [29]. This branching ratio of χ_1 is a fit.

widths of the P-wave charmonia be brought in range of the experimental measurements. It would be better to show this in the modified hard scattering scheme which has the advantage of the dynamical setting of renormalization scales by the process itself. But due to the complexity of the calculations, we have to revert back to the standard scheme. Remembering this dynamical setting of scales is only possible if the Landau pole in α_s is suppressed by the Sudakov factor or better yet if it is not present at all. This suggests the use of one of the analytic models for α_s which are free from the problem of the Landau pole [31, 32, 33, 34]. The one suggested in [33] is particularly appealing because of its relative simplicity. By combining $\alpha_s^{\text{analytic}}$ with the standard hard scattering approach, a simpler scheme than the modified one can be constructed, but nevertheless still preserving the best features of that scheme. Under the new scheme, the amplitude would be given by

$$\mathcal{M} \sim f_{\chi_J} \phi_{\chi_J}(x) \otimes f_N \phi_N(x) \otimes f_{\bar{N}} \phi_{\bar{N}}(x) \otimes T_H(x, \alpha_s^{\text{analytic}}(x)). \quad (56)$$

We have also tried using this semi-modified scheme and again both colour singlet and octet must be included. The details will be given elsewhere [35]. A somewhat similar use of this analytic α_s model in exclusive process to study pion form factors can be found in [36].

Thus having satisfied ourselves with the genuine necessity and the correctness of the inclusion of the colour octet state in P-wave charmonium decays, we can now general-

ize the arguments to even higher wave quarkonia. Remembering that the P-wave $Q\bar{Q}$ wavefunction has a $1/M$ suppression due to angular momentum, so one can deduce in a straight forward manner that for a D-wave, the wavefunction would be doubly suppressed by $1/M^2$ in relation to a S-wave. Then to calculate the exclusive decay of a D-wave quarkonium, one would need to include not only the colour singlet valence state and the next higher colour octet state now with the heavy fermions in a P-wave, but the next-next higher state must also be included for a consistent calculation.

Finally as mentioned in the introduction, nucleon wavefunction constructed from QCD sum rules has large disagreement with the magnetic form factor measurements below 50 GeV². Therefore while lacking an alternative method to derive wavefunction in a fundamental way, we will have to satisfy with phenomenological constructions. We have shown together with [11] that the so-constructed wavefunction and its generalization to the flavour octet and decuplet baryons provide a set of reasonable model wavefunctions. They would no doubt provide a useful basis for future study of other exclusive processes involving baryons at moderate Q^2 .

Acknowledgments

The author would like to thank most of all P. Kroll for introducing him to the very interesting subjects of the hard scattering scheme and the colour octet picture of quarkonium. The author benefited greatly from his initial guidance of this research and from many useful discussions. The author also thanks the computational physics group of K. Schilling in Fachbereich Theoretische Physik, Universität Wuppertal for using their valuable computer resources and for the Nuclear and Particle Physics Section and IASA institute at the University of Athens for kind hospitality where part of this work was done. All algebras, including those of the Dirac and colour, have been performed with the computer program FORM v1.0. written by J.A.M. Vermaseren. This work was supported by the European Training and Mobility of Researchers Programme under contract no. ERB-FMRX-CT96-0008.

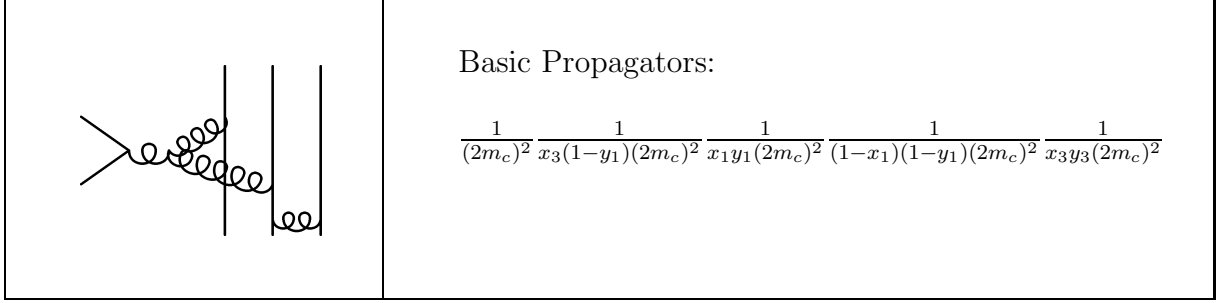


Figure 7: Basic graph of Group 1

A Appendix: Basic Graphs And Contributions For colour octet

A.1 Group 1

I.P.	Num. for graphs of Group 1 with ($\lambda_1, \lambda_2, \lambda_3$) = (+, +, -)	
	J=1	J=2
U3	\emptyset	\emptyset
L3	$\sqrt{2}(x_3 - z)(y_3 - z)(1 + y_1 - z)$	
U2	$-\frac{4\sqrt{2}}{3}x_3\{(x_2 - z)(1 + y_1 - z) - (-1)^J 2z(x_1 - y_1)\}$	
M2	$-\frac{4\sqrt{2}}{3}x_3(x_3 - z)(1 + y_1 - z)$	
L2	$\frac{\sqrt{2}}{3}(x_3 - z)(y_2 - z)(1 + y_1 - z)$	
U1	$\frac{4\sqrt{2}}{3}x_3\{(x_1 - z)(1 - y_1 - 2z) + (-1)^J z(x_1 - y_1 + 3(1 - z))\}$	
L1	$-\frac{4\sqrt{2}}{3}x_3\{(1 + y_1 - 2z)(y_1 - z) - (-1)^J z(1 - 2y_1 + z)\}$	
G3	$-\sqrt{2}(x_3 - y_3)(x_3 - z)(1 + y_1 - z)$	
G2	$\frac{4\sqrt{2}}{3}x_3\{2(1 - z^2) - y_1(3 + y_1 - 6z) + x_1(3 - y_1 - 2z) - (-1)^J 2(x_1 - y_1)(1 - y_1 - 2z)\}$	
G1	$\frac{4\sqrt{2}}{3}x_3\{2(x_1 - y_1)(1 + y_1 - 2z) + (-1)^J (2z(2 - z) + x_1(1 - y_1 + 2z) + y_1(3 - y_1 - 6z))\}$	
4G	\emptyset	$-\frac{16\sqrt{2}}{3}x_3$

Table 5: (a) Numerators of the graphs of group 1 with helicity (+, +, -).

I.P.	Num. for graphs of Group 1 with ($\lambda_1, \lambda_2, \lambda_3$) = (+, -, +)	
	J=1	J=2
U3	\emptyset	\emptyset
L3	(+, +, -) + (-, +, +)	
U2	$-\frac{4\sqrt{2}}{3}x_3(x_2 - z)(1 + y_1 - z)$	
M2	$-\frac{4\sqrt{2}}{3}x_3\{(x_3 - z)(1 + y_1 - z) + (-1)^J 2(x_1 - y_1)(1 - y_1 - z)\}$	
L2	$\frac{\sqrt{2}}{3}(x_3 - z)(y_2 - z)(1 + y_1 - z)$	
U1	$\frac{4\sqrt{2}}{3}x_3\{(x_1 - z)(1 - y_1 - 2z) + (-1)^J z(x_1 - y_1 + 3(1 - z))\}$	
L1	$-\frac{4\sqrt{2}}{3}x_3\{(1 + y_1 - 2z)(y_1 - z) - (-1)^J z(1 - 2y_1 + z)\}$	
G3	(+, +, -) + (-, +, +)	
G2	$\frac{4\sqrt{2}}{3}x_3\{2(1 - z^2) - y_1(3 + y_1 - 6z) + x_1(3 - y_1 - 2z) - (-1)^J 2(x_1 - y_1)(1 - y_1 - 2z)\}$	
G1	$\frac{4\sqrt{2}}{3}x_3\{2(x_1 - y_1)(1 + y_1 - 2z) + (-1)^J (2z(2 - z) + x_1(1 - y_1 + 2z) + y_1(3 - y_1 - 6z))\}$	
4G	\emptyset	$-\frac{16\sqrt{2}}{3}x_3$

Table 5: (b) Numerators of the graphs of group 1 with helicity (+, -, +).

I.P.	Num. for graphs of Group 1 with ($\lambda_1, \lambda_2, \lambda_3$) = (-, +, +)		X-Prop.
	J=1	J=2	
U3	\emptyset	\emptyset	n. g.
L3	$-(-1)^J 2\sqrt{2}z(x_1 - y_1)(1 - y_1 - z)$		$\frac{1}{-z(y_3 - z)(2m_c)^2}$
U2	\emptyset	\emptyset	$\frac{1}{-z(x_2 - z)(2m_c)^2}$
M2	\emptyset	\emptyset	$\frac{1}{x_3(1 - y_1)(2m_c)^2}$
L2	$(-1)^J \frac{2\sqrt{2}}{3}z(x_1 - y_1)(1 - y_1 - z)$		$\frac{1}{-z(y_2 - z)(2m_c)^2}$
U1	\emptyset	\emptyset	$\frac{1}{-z(x_1 - z)(2m_c)^2}$
L1	\emptyset	\emptyset	$\frac{1}{-z(y_1 - z)(2m_c)^2}$
G3	$-(-1)^J \sqrt{2}(x_1 - y_1)(x_3 + z)(1 - y_1 - z)$		$\frac{1}{x_3 y_3 (2m_c)^2}$
G2	\emptyset	\emptyset	$\frac{1}{(1 - x_1)(1 - y_1)(2m_c)^2}$
G1	\emptyset	\emptyset	$\frac{1}{x_1 y_1 (2m_c)^2}$
4G	\emptyset	\emptyset	$\frac{1}{(2m_c)^2}$

Table 5: (c) Numerators and the additional propagators of the graphs of group 1 with helicity (-, +, +).

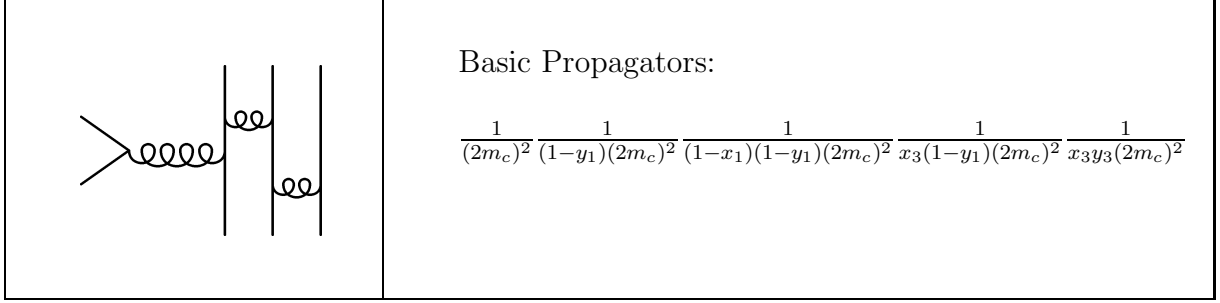


Figure 8: Basic graph of Group 2

A.2 Group 2 and Group 2'

A.2.1 Group 2

I.P.	Num. for graphs of Group 2 with $(\lambda_1, \lambda_2, \lambda_3)$			
	$(+, +, -)$		$(+, -, +)$	
	J=1	J=2	J=1	J=2
U3	\emptyset	\emptyset	\emptyset	\emptyset
L3	\emptyset	\emptyset	$-(-1)^J \frac{32\sqrt{2}}{27} z(1-y_1-z)^2$	
U2	$(-1)^J \frac{40\sqrt{2}}{27} x_3 z(1-y_1-z)$		\emptyset	\emptyset
M2	\emptyset	\emptyset	$-(-1)^J \frac{32\sqrt{2}}{27} x_3(1-y_1-z)^2$	
L2	\emptyset	\emptyset	\emptyset	\emptyset
U1	$(-1)^J \frac{8\sqrt{2}}{27} x_3 z(1-y_1-z)$			
M1	\emptyset	\emptyset	\emptyset	\emptyset
L1	\emptyset	\emptyset	\emptyset	\emptyset
G3	\emptyset	\emptyset	\emptyset	\emptyset
G2	$\frac{4\sqrt{2}}{3} x_3 \{ (1-z)(2(1-y_1)-z) - (-1)^J (1-y_1-2z)(1-y_1-z) \}$			

Table 6: (a) Numerators of the graphs of group 2 with helicity $(+, +, -)$ and $(+, -, +)$.

I.P.	Num. for graphs of Group 2 with $(\lambda_1, \lambda_2, \lambda_3) = (-, +, +)$		X-Prop.
	J=1	J=2	
U3	\emptyset	\emptyset	n. g.
L3	$-(-1)^J \frac{32\sqrt{2}}{27} z(1 - y_1 - z)^2$		$\frac{1}{-z(y_3-z)(2m_c)^2}$
U2	\emptyset	\emptyset	$\frac{1}{-z(x_2-z)(2m_c)^2}$
M2	\emptyset	\emptyset	$\frac{1}{x_3(1-y_1)(2m_c)^2}$
L2	$(-1)^J \frac{32\sqrt{2}}{27} z(1 - y_1 - z)^2$		$\frac{1}{-z(y_2-z)(2m_c)^2}$
U1	\emptyset	\emptyset	$\frac{1}{-z(x_1-z)(2m_c)^2}$
M1	\emptyset	\emptyset	n. g.
L1	\emptyset	\emptyset	n. g.
G3	\emptyset	\emptyset	n. g.
G2	\emptyset	\emptyset	$\frac{1}{(1-x_1)(1-y_1)(2m_c)^2}$

Table 6: (b) Numerators and the additional propagators of the graphs of group 2 with helicity $(-, +, +)$.

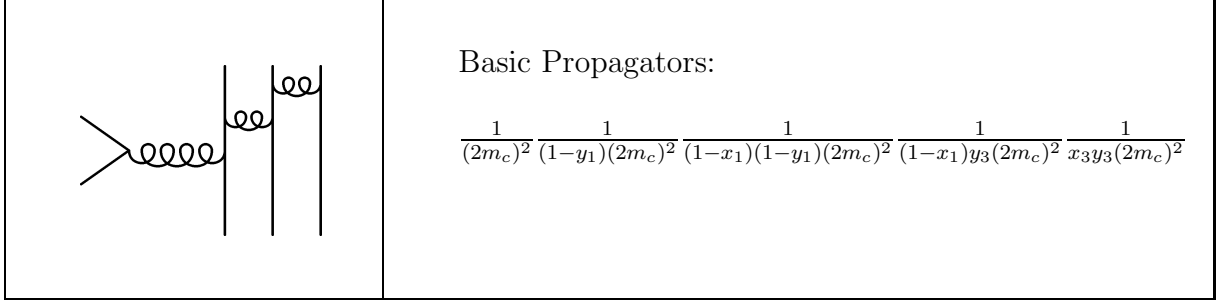


Figure 9: Basic graph of Group 2'

A.2.2 Group 2'

I.P.	Num. for graphs of Group 2' with ($\lambda_1, \lambda_2, \lambda_3$) = (+, +, -)	
	J=1	J=2
U3	$\frac{22\sqrt{2}}{27}(1-z)(x_3-z)(y_3-z)$	
L3	$-\frac{32\sqrt{2}}{27}(1-z)(y_3-z)^2$	
U2	$-\frac{14\sqrt{2}}{27}(1-z)(x_2-z)(y_3-z)$	
M2	$-\frac{40\sqrt{2}}{27}y_3(1-z)(y_3-z)$	
L2	$-\frac{32\sqrt{2}}{27}y_3\{(1-z)(y_2-z) + (-1)^J z(1-y_1-z)\}$	
U1	$-\frac{8\sqrt{2}}{27}y_3(1-z)(x_1-z)$	
M1	$\frac{64\sqrt{2}}{27}y_3\{(1-z) - (-1)^J(1-y_1-z)\}$	
L1	$\frac{64\sqrt{2}}{27}y_3\{y_1-z + (-1)^J z\}$	
G3	$2\sqrt{2}(1-z)(x_3-y_3)(y_3-z)$	
G2	$-\frac{4\sqrt{2}}{3}y_3\{(1-z)(x_1-y_1-3z) - (-1)^J(1-x_1-2z)(1-y_1-z)\}$	

Table 6: (a') Numerators of the graphs of group 2' with helicity (+, +, -).

I.P.	Num. for graphs of Group 2' with ($\lambda_1, \lambda_2, \lambda_3$) = (+, -, +)	
	J=1	J=2
U3	(+, +, -) + (-, +, +)	
L3	$-\frac{32\sqrt{2}}{27}(1-z)(y_3-z)^2$	
U2	$-\frac{14\sqrt{2}}{27}(1-z)(x_2-z)(y_3-z)$	
M2	$-\frac{40\sqrt{2}}{27}y_3\{(1-z)(y_3-z) - (-1)^J(1-x_1-z)(1-y_1-z)\}$	
L2	$-\frac{32\sqrt{2}}{27}y_3(1-z)(y_2-z)$	
U1	$-\frac{8\sqrt{2}}{27}y_3(1-z)(x_1-z)$	
M1	$\frac{64\sqrt{2}}{27}y_3\{(1-z) - (-1)^J(1-y_1-z)\}$	
L1	$\frac{64\sqrt{2}}{27}y_3\{y_1-z + (-1)^Jz\}$	
G3	(+, +, -) + (+, -, +)	
G2	$-\frac{4\sqrt{2}}{3}y_3\{(1-z)(x_1-y_1-3z) - (-1)^J(1-x_1-2z)(1-y_1-z)\}$	

Table 6: (b') Numerators of the graphs of group 2' with helicity (+, -, +).

I.P.	Num. for graphs of Group 2' with ($\lambda_1, \lambda_2, \lambda_3$) = (-, +, +)		X-Prop.
	J=1	J=2	
U3	$(-1)^J \frac{22\sqrt{2}}{27} z(1-x_1-z)(1-y_1-z)$		$\frac{1}{-z(x_3-z)(2m_c)^2}$
L3	\emptyset	\emptyset	$\frac{1}{-z(y_3-z)(2m_c)^2}$
U2	$(-1)^J \frac{14\sqrt{2}}{27} z(1-x_1-z)(1-y_1-z)$		$\frac{1}{-z(x_2-z)(2m_c)^2}$
M2	\emptyset	\emptyset	$\frac{1}{(1-x_1)y_3(2m_c)^2}$
L2	\emptyset	\emptyset	$\frac{1}{-z(y_2-z)(2m_c)^2}$
U1	\emptyset	\emptyset	$\frac{1}{-z(x_1-z)(2m_c)^2}$
M1	\emptyset	\emptyset	$\frac{1}{(1-y_1)(2m_c)^2}$
L1	\emptyset	\emptyset	$\frac{1}{-z(y_1-z)(2m_c)^2}$
G3	$(-1)^J \sqrt{2}(1-x_1-z)(1-y_1-z)(y_3+z)$		$\frac{1}{x_3y_3(2m_c)^2}$
G2	\emptyset	\emptyset	$\frac{1}{(1-x_1)(1-y_1)(2m_c)^2}$

Table 6: (c') Numerators and the additional propagators of the graphs of group 2' with helicity (-, +, +).

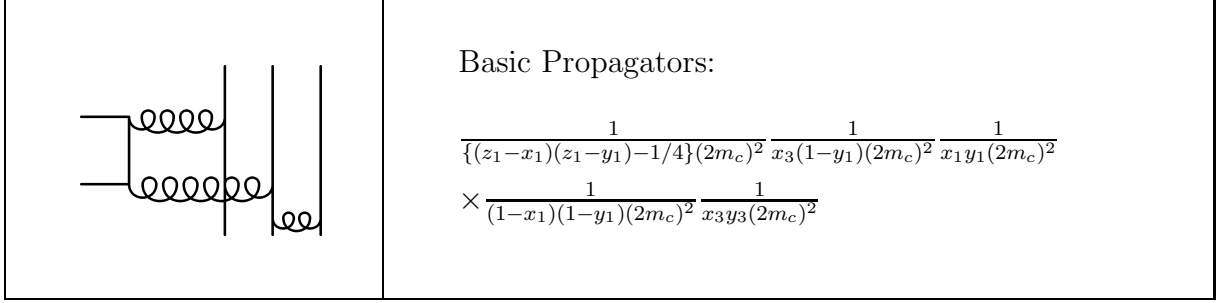


Figure 10: Basic graph of Group 3

A.3 Group 3

I.P.	Num. for graphs of Group 3 with ($\lambda_1, \lambda_2, \lambda_3$) = (+, +, -)	
	J=1	J=2
U3	$-\frac{10\sqrt{2}}{27}(x_3 - z)^2(2y_1 + z)$	
L3	$\frac{8\sqrt{2}}{27}(x_3 - z)(y_3 - z)(2y_1 + z)$	
U2	$-\frac{4\sqrt{2}}{27}x_3\{(x_2 - z)(2y_1 + z) - (-1)^J 2z(x_1 - y_1)\}$	
M2	$-\frac{14\sqrt{2}}{27}x_3(x_3 - z)(2y_1 + z)$	
L2	$-\frac{4\sqrt{2}}{27}(x_3 - z)(y_2 - z)(2y_1 + z)$	
U1	$\frac{14\sqrt{2}}{27}x_3\{(x_1 - z)(2y_1 - z) + (-1)^J 2z\}$	
L1	$-\frac{4\sqrt{2}}{27}x_3\{(2y_1 - z)(y_1 - z) - (-1)^J 2z(1 - 2y_1 + z)\}$	
G3	$-\frac{2\sqrt{2}}{3}(x_3 - z)(x_3 - y_3)(2y_1 + z)$	
G2	$-\frac{\sqrt{2}}{3}x_3\{(x_1 + y_1 - 2z)(2y_1 + z) - 2(2x_1 + z) + (-1)^J(x_1 - y_1)(1 - y_1 - 2z)\}$	
G1	$\frac{2\sqrt{2}}{3}x_3\{(x_1 - y_1)(2y_1 - z) - (-1)^J((x_1 + z)(2y_1 - z) - (x_1 + y_1 + 2z))\}$	
Q	$-\frac{\sqrt{2}}{27}x_3\{\frac{1}{2}(2y_1 + z)(2y_1 - z) - (x_1 + y_1 + z) + (-1)^J(\frac{1}{2}(2x_1 + z)(2y_1 - z) - (x_1 + y_1 + z))\}$	

Table 7: (a) Numerators of the graphs of group 3 with helicity (+, +, -).

I.P.	Num. for graphs of Group 3 with ($\lambda_1, \lambda_2, \lambda_3$) = (+, -, +)	
	J=1	J=2
U3	$-\frac{10\sqrt{2}}{27}(x_3 - z)^2(2y_1 + z)$	
L3	$\frac{8\sqrt{2}}{27}\{(x_3 - z)(y_3 - z)(2y_1 + z) - (-1)^J 2z(x_1 - y_1)(1 - y_1 - z)\}$	
U2	$-\frac{4\sqrt{2}}{27}x_3(x_2 - z)(2y_1 + z)$	
M2	$-\frac{14\sqrt{2}}{27}x_3\{(x_3 - z)(2y_1 + z) + (-1)^J 2z(x_1 - y_1)(1 - y_1 - z)\}$	
L2	$-\frac{4\sqrt{2}}{27}(x_3 - z)(y_2 - z)(2y_1 + z)$	
U1	$\frac{14\sqrt{2}}{27}x_3\{(x_1 - z)(2y_1 - z) + (-1)^J 2z\}$	
L1	$-\frac{4\sqrt{2}}{27}x_3\{(2y_1 - z)(y_1 - z) - (-1)^J 2z(1 - 2y_1 + z)\}$	
G3	$(+, +, -) + (-, +, +)$	
G2	$-\frac{\sqrt{2}}{3}x_3\{(x_1 + y_1 - 2z)(2y_1 + z) - 2(2x_1 + z) + (-1)^J(x_1 - y_1)(1 - y_1 - 2z)\}$	
G1	$\frac{2\sqrt{2}}{3}x_3\{(x_1 - y_1)(2y_1 - z) - (-1)^J((x_1 + z)(2y_1 - z) - (x_1 + y_1 + 2z))\}$	
Q	$-\frac{\sqrt{2}}{27}x_3\{\frac{1}{2}(2y_1 + z)(2y_1 - z) - (x_1 + y_1 + z) + (-1)^J(\frac{1}{2}(2x_1 + z)(2y_1 - z) - (x_1 + y_1 + z))\}$	

Table 7: (b) Numerators of the graphs of group 3 with helicity (+, -, +).

I.P.	Num. for graphs of Group 3 with ($\lambda_1, \lambda_2, \lambda_3$) = (-, +, +)		X-Prop.
	J=1	J=2	
U3	\emptyset	\emptyset	$\frac{1}{-z(x_3 - z)(2m_c)^2}$
L3	$-(-1)^J \frac{16\sqrt{2}}{27} z(x_1 - y_1)(1 - y_1 - z)$		$\frac{1}{-z(y_3 - z)(2m_c)^2}$
U2	\emptyset	\emptyset	$\frac{1}{-z(x_2 - z)(2m_c)^2}$
M2	\emptyset	\emptyset	$\frac{1}{x_3(1 - y_1)(2m_c)^2}$
L2	$-(-1)^J \frac{8\sqrt{2}}{27} z(x_1 - y_1)(1 - y_1 - z)$		$\frac{1}{-z(y_2 - z)(2m_c)^2}$
U1	\emptyset	\emptyset	$\frac{1}{-z(x_1 - z)(2m_c)^2}$
L1	\emptyset	\emptyset	$\frac{1}{-z(y_1 - z)(2m_c)^2}$
G3	$-(-1)^J \frac{2\sqrt{2}}{3}(x_3 + z)(x_1 - y_1)(1 - y_1 - z)$		$\frac{1}{x_3 y_3 (2m_c)^2}$
G2	\emptyset	\emptyset	$\frac{1}{(1 - x_1)(1 - y_1)(2m_c)^2}$
G1	\emptyset	\emptyset	$\frac{1}{x_1 y_1 (2m_c)^2}$
Q	\emptyset	\emptyset	$\frac{1}{[(x_1 - z_1)(y_1 - z_1) - 1/4](2m_c)^2}$

Table 7: (c) Numerators and the additional propagators of the graphs of group 3 with helicity (-, +, +).

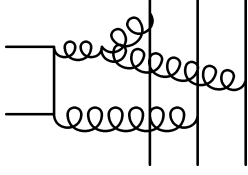
	<p>Basic Propagators:</p> $\frac{1}{\{(z_2-x_2)(z_2-y_2)-1/4\}(2m_c)^2} \frac{1}{(1-x_2)(1-y_2)(2m_c)^2+\rho^2} \frac{1}{x_1y_1(2m_c)^2}$ $\times \frac{1}{x_2y_2(2m_c)^2} \frac{1}{x_3y_3(2m_c)^2}$
---	--

Figure 11: Basic graph of Group 4

A.4 Group 4

I.P.	Num. for graphs of Group 4 with $(\lambda_1, \lambda_2, \lambda_3)$			
	$(+, +, -)$		$(+, -, +)$	
	J=1	J=2	J=1	J=2
U3	$-\frac{\sqrt{2}}{3}(x_3 - z) \{ (x_1 - x_3 + z) + (y_1 - y_3 + z) - 2(x_1 - x_3 + z)(z_2 - y_2) - 2(y_1 - y_3 + z)(z_2 - x_2) \}$		$(-1)^J \frac{2\sqrt{2}}{3} z(x_2 - y_2)(2x_1 + x_3 - z)$	
L3	$\frac{\sqrt{2}}{12}(y_3 - z) \{ (x_1 - x_3 + z) + (y_1 - y_3 + z) - 2(x_1 - x_3 + z)(z_2 - y_2) - 2(y_1 - y_3 + z)(z_2 - x_2) \}$		$(-1)^J \frac{\sqrt{2}}{6} z(x_2 - y_2)(2y_1 + y_3 - z)$	
U2	\emptyset	\emptyset	\emptyset	\emptyset
L2	\emptyset	\emptyset	\emptyset	\emptyset
U1	$(+, -, +) + (-, +, +)$		$(-1)^J \frac{2\sqrt{2}}{3} z(x_2 - y_2)(x_1 + 2x_3 - z)$	
L1	$(+, -, +) + (-, +, +)$		$(-1)^J \frac{\sqrt{2}}{6} z(x_2 - y_2)(y_1 + 2y_3 - z)$	
G3	$-\frac{5\sqrt{2}}{12}(x_3 - y_3) \{ (x_1 - x_3 + z) + (y_1 - y_3 + z) - 2(x_1 - x_3 + z)(z_2 - y_2) - 2(y_1 - y_3 + z)(z_2 - x_2) \}$		$(-1)^J \frac{5\sqrt{2}}{12} (x_2 - y_2) \times \{ (2x_1 + x_3 - z)(y_3 + z) (2y_1 + y_3 - z)(x_3 + z) \}$	
G2	\emptyset	\emptyset	\emptyset	\emptyset
G1	$(+, -, +) + (-, +, +)$		$(-1)^J \frac{5\sqrt{2}}{12} (x_2 - y_2) \times \{ (2x_3 + x_1 - z)(y_1 + z) (2y_3 + y_1 - z)(x_1 + z) \}$	
GR	\emptyset	\emptyset	\emptyset	\emptyset
4G	$-\frac{5}{\sqrt{2}}(x_2 - y_2)$	$-\frac{5}{3\sqrt{2}}(x_2 - y_2)$	$-(-1)^J \frac{5\sqrt{2}}{3} (x_2 - y_2)$	
Q	\emptyset	\emptyset	\emptyset	\emptyset

Table 8: (a) Numerators of the graphs of group 4 with helicity $(+, +, -)$ and $(+, -, +)$.

I.P.	Num. for graphs of Group 4 with $(\lambda_1, \lambda_2, \lambda_3) = (-, +, +)$		X-Prop.
	J=1	J=2	
U3	$(+, +, -) + (+, -, +)$		$\frac{1}{-z(x_3-z)(2m_c)^2}$
L3	$(+, +, -) + (+, -, +)$		$\frac{1}{-z(y_3-z)(2m_c)^2}$
U2	\emptyset	\emptyset	n. g.
L2	\emptyset	\emptyset	n. g.
U1	$-\frac{\sqrt{2}}{3}(x_1 - z)\{ (x_3 - x_1 + z) + (y_3 - y_1 + z) - 2(x_3 - x_1 + z)(z_2 - y_2) - 2(y_3 - y_1 + z)(z_2 - x_2) \}$		$\frac{1}{-z(x_1-z)(2m_c)^2}$
L1	$\frac{\sqrt{2}}{12}(y_1 - z)\{ (x_3 - x_1 + z) + (y_3 - y_1 + z) - 2(x_3 - x_1 + z)(z_2 - y_2) - 2(y_3 - y_1 + z)(z_2 - x_2) \}$		$\frac{1}{-z(y_1-z)(2m_c)^2}$
G3	$(+, +, -) + (+, -, +)$		$\frac{1}{x_3 y_3 (2m_c)^2}$
G2	\emptyset	\emptyset	n. g.
G1	$-\frac{5\sqrt{2}}{12}(x_1 - y_1)\{ (x_3 - x_1 + z) + (y_3 - y_1 + z) - 2(x_3 - x_1 + z)(z_2 - y_2) - 2(y_3 - y_1 + z)(z_2 - x_2) \}$		$\frac{1}{x_1 y_1 (2m_c)^2}$
GR	\emptyset	\emptyset	n. g.
4G	$-\frac{5}{\sqrt{2}}(x_2 - y_2)$	$-\frac{5}{3\sqrt{2}}(x_2 - y_2)$	$\frac{1}{(2m_c)^2}$
Q	\emptyset	\emptyset	n. g.

Table 8: (b) Numerators and the additional propagators of the graphs of group 4 with helicity $(-, +, +)$.

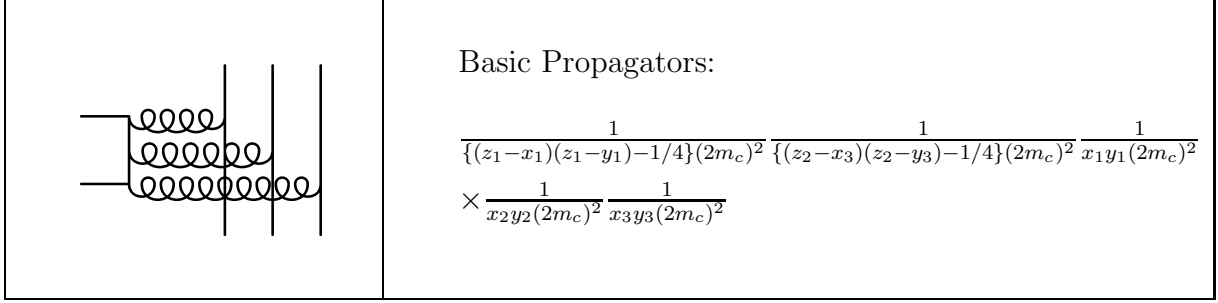


Figure 12: Basic graph of Group 5

A.5 Group 5

I.P.	Num. for graphs of Group 5 with ($\lambda_1, \lambda_2, \lambda_3$) = (+, +, -)	
	J=1	J=2
U3	\emptyset	\emptyset
L3	\emptyset	\emptyset
U2	$-(-1)^J \frac{\sqrt{2}}{12} z(2x_1 + z)(2x_3 + z)$	
L2	$-(-1)^J \frac{\sqrt{2}}{12} z(2y_1 + z)(2y_3 + z)$	
U1	$(-1)^J \frac{\sqrt{2}}{4} z \{1 - 2x_2 - 4(x_2 + x_3 - z_1)(y_3 - z_1)\}$	
L1	$-(-1)^J \frac{\sqrt{2}}{6} z \{1 - 2y_2 - 4(y_2 + y_3 - z_1)(x_3 - z_1)\}$	
G3	\emptyset	\emptyset
G2	\emptyset	\emptyset
G1	$-(-1)^J \frac{5}{12\sqrt{2}} \{ (x_1 - y_1)(1 - 4(x_3 - z_1)(y_3 - z_1))$ $+ 2x_2(2y_3 + z)(y_1 + z)$ $- 2y_2(2x_3 + z)(x_1 + z) \}$	
UQ	$-(-1)^J \frac{5\sqrt{2}}{108} \{ (x_3 - y_3) - 2z(x_2 - y_2) + 4(x_1 - y_1)(1 - z_1)^2$ $- 4(x_1(1 - x_3) - x_2 z_1)(1 - y_1 - z_1)$ $+ 4(y_1(1 - y_3) - y_2 z_1)(1 - x_1 - z_1) \}$	
LQ	\emptyset	\emptyset

Table 9: (a) Numerators of the graphs of group 5 with helicity (+,+,−).

I.P.	Num. for graphs of Group 5 with ($\lambda_1, \lambda_2, \lambda_3$) = (+, -, +)	
	J=1	J=2
U3	$-\frac{\sqrt{2}}{6} \{ 2(x_3 - z)[1 - x_2 - y_2 - 2(1 - x_3 - z_1)(y_1 - z_1) - 2(1 - y_3 - z_1)(x_1 - z_1)] + (-1)^J z [1 - 2x_2 - 4(1 - x_3 - z_1)(y_1 - z_1)] \}$	
L3	$\frac{\sqrt{2}}{4} \{ 2(y_3 - z)[1 - x_2 - y_2 - 2(1 - x_3 - z_1)(y_1 - z_1) - 2(1 - y_3 - z_1)(x_1 - z_1)] + (-1)^J z [1 - 2y_2 - 4(1 - y_3 - z_1)(x_1 - z_1)] \}$	
U2	$-\frac{\sqrt{2}}{6} (x_2 - z) \{ 1 - (x_2 + y_2 - 2z) + 2(x_3 - z_1)(y_1 - z_1) + 2(y_3 - z_1)(x_1 - z_1) \}$	
L2	$-\frac{\sqrt{2}}{6} (y_2 - z) \{ 1 - (x_2 + y_2 - 2z) + 2(x_3 - z_1)(y_1 - z_1) + 2(y_3 - z_1)(x_1 - z_1) \}$	
U1	$\frac{\sqrt{2}}{4} \{ 2(x_1 - z)[1 - x_2 - y_2 - 2(1 - x_1 - z_1)(y_3 - z_1) - 2(1 - y_1 - z_1)(x_3 - z_1)] + (-1)^J z [1 - 2x_2 - 4(1 - x_1 - z_1)(y_3 - z_1)] \}$	
L1	$-\frac{\sqrt{2}}{6} \{ 2(y_1 - z)[1 - x_2 - y_2 - 2(1 - x_1 - z_1)(y_3 - z_1) - 2(1 - y_1 - z_1)(x_3 - z_1)] + (-1)^J z [1 - 2y_2 - 4(1 - y_1 - z_1)(x_3 - z_1)] \}$	
G3	$-\frac{5}{12\sqrt{2}} \{ 4(x_3 - y_3)[1 - y_2 - x_2(2y_1 + z) - 2(x_1 - z_1)(y_1 - y_3 + z)] - (-1)^J [2z(x_2(2y_1 + z) - y_2(2x_1 + z)) + x_3(1 - 2y_2 - 4(x_1 - z_1)(1 - y_3 - z_1)) - y_3(1 - 2x_2 - 4(y_1 - z_1)(1 - x_3 - z_1))] \}$	
G2	\emptyset	\emptyset
G1	$\frac{5}{12\sqrt{2}} \{ 4(x_1 - y_1)[1 - y_2 - x_2(2y_3 + z) + 2(x_3 - z_1)(y_1 - y_3 - z)] - (-1)^J [2z(x_2(2y_3 + z) - y_2(2x_3 + z)) + x_1(1 - 2y_2 - 4(x_3 - z_1)(1 - y_1 - z_1)) - y_1(1 - 2x_2 - 4(y_3 - z_1)(1 - x_1 - z_1))] \}$	
UQ	$-\frac{5\sqrt{2}}{108} \{ z(2+z)(x_1 - y_1) + (z(2-z) + 2(x_1 + y_1))(x_2 - y_2) + 4(z_1 - y_3)x_1^2 - 4(z_1 - x_3)y_1^2 \}$	
LQ	$\frac{5\sqrt{2}}{108} \{ z(2+z)(x_3 - y_3) + (z(2-z) + 2(x_3 + y_3))(x_2 - y_2) + 4(z_1 - y_1)x_3^2 - 4(z_1 - x_1)y_3^2 \}$	

Table 9: (b) Numerators of the graphs of group 5 with helicity (+, -, +).

I.P.	Num. for graphs of Group 5 with ($\lambda_1, \lambda_2, \lambda_3$) = (-, +, +)		X-Prop.
	J=1	J=2	
U3	$-(-1)^J \frac{\sqrt{2}}{6} z \{1 - 2x_2 - 4(x_1 + x_2 - z_1)(y_1 - z_1)\}$		$\frac{1}{-z(x_3 - z)(2m_c)^2}$
L3	$(-1)^J \frac{\sqrt{2}}{4} z \{1 - 2y_2 - 4(y_1 + y_2 - z_1)(x_1 - z_1)\}$		$\frac{1}{-z(y_3 - z)(2m_c)^2}$
U2	$-(-1)^J \frac{\sqrt{2}}{12} z (2x_1 + z)(2x_3 + z)$		$\frac{1}{-z(x_2 - z)(2m_c)^2}$
L2	$-(-1)^J \frac{\sqrt{2}}{12} z (2y_1 + z)(2y_3 + z)$		$\frac{1}{-z(y_2 - z)(2m_c)^2}$
U1	\emptyset	\emptyset	$\frac{1}{-z(x_1 - z)(2m_c)^2}$
L1	\emptyset	\emptyset	$\frac{1}{-z(y_1 - z)(2m_c)^2}$
G3	$(-1)^J \frac{5}{12\sqrt{2}} \{ (x_3 - y_3)(1 - 4(x_1 - z_1)(y_1 - z_1))$ $+ 2x_2(2y_1 + z)(y_3 + z)$ $- 2y_2(2x_1 + z)(x_3 + z) \}$		$\frac{1}{x_3 y_3 (2m_c)^2}$
G2	\emptyset	\emptyset	n. g.
G1	\emptyset	\emptyset	$\frac{1}{x_1 y_1 (2m_c)^2}$
UQ	\emptyset	\emptyset	$\frac{1}{[(x_1 - z_1)(y_1 - z_1) - 1/4](2m_c)^2}$
LQ	$(-1)^J \frac{5\sqrt{2}}{108} \{ (x_1 - y_1) - 2z(x_2 - y_2) + 4(x_3 - y_3)(1 - z_1)^2$ $- 4(x_3(1 - x_1) - x_2 z_1)(1 - y_3 - z_1)$ $+ 4(y_3(1 - y_1) - y_2 z_1)(1 - x_3 - z_1) \}$		$\frac{1}{[(x_3 - z_1)(y_3 - z_1) - 1/4](2m_c)^2}$

Table 9: (c) Numerators and the additional propagators of the graphs of group 5 with helicity (-,+,+).

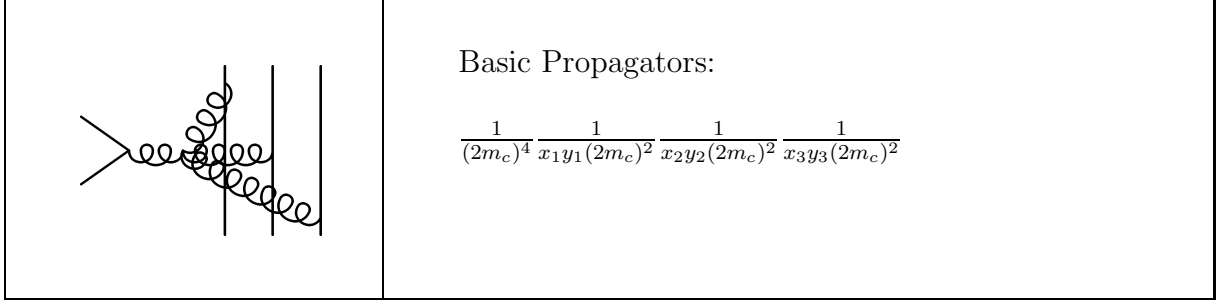


Figure 13: Basic graph of Group 6

A.6 Group 6

I.P.	Num. for graphs of Group 6 with $(\lambda_1, \lambda_2, \lambda_3)$			
	$(+, +, -)$		$(+, -, +)$	
	J=1	J=2	J=1	J=2
U3	$2\sqrt{2}(x_3 - z)$		$-\sqrt{2}\{x_3 - z + (-1)^J 2z\}$	
L3	$2\sqrt{2}(y_3 - z)$		$-\sqrt{2}\{y_3 - z + (-1)^J 2z\}$	
U2	$-\sqrt{2}\{x_2 - z + (-1)^J 2z\}$		$2\sqrt{2}(x_2 - z)$	
L2	$-\sqrt{2}\{y_2 - z + (-1)^J 2z\}$		$2\sqrt{2}(y_2 - z)$	
U1	$-\sqrt{2}\{x_1 - z + (-1)^J 2z\}$			
L1	$-\sqrt{2}\{y_1 - z + (-1)^J 2z\}$			
G3	\emptyset	\emptyset	\emptyset	\emptyset
G2	\emptyset	\emptyset	\emptyset	\emptyset
G1	\emptyset	\emptyset	\emptyset	\emptyset

Table 10: (a) Numerators of the graphs of group 6 with helicity $(+, +, -)$ and $(+, -, +)$.

I.P.	Num. for graphs of Group 6 with $(\lambda_1, \lambda_2, \lambda_3) = (-, +, +)$		X-Prop.
	J=1	J=2	
U3	$-\sqrt{2}\{x_3 - z + (-1)^J 2z\}$		$\frac{1}{-z(x_3-z)(2m_c)^2}$
L3	$-\sqrt{2}\{y_3 - z + (-1)^J 2z\}$		$\frac{1}{-z(y_3-z)(2m_c)^2}$
U2	$-\sqrt{2}\{x_2 - z + (-1)^J 2z\}$		$\frac{1}{-z(x_2-z)(2m_c)^2}$
L2	$-\sqrt{2}\{y_2 - z + (-1)^J 2z\}$		$\frac{1}{-z(y_2-z)(2m_c)^2}$
U1	$2\sqrt{2}(x_1 - z)$		$\frac{1}{-z(x_1-z)(2m_c)^2}$
L1	$2\sqrt{2}(y_1 - z)$		$\frac{1}{-z(y_1-z)(2m_c)^2}$
G3	\emptyset	\emptyset	n. g.
G2	\emptyset	\emptyset	n. g.
G1	\emptyset	\emptyset	n. g.

Table 10: (b) Numerators and the additional propagators of the graphs of group 6 with helicity $(-, +, +)$.

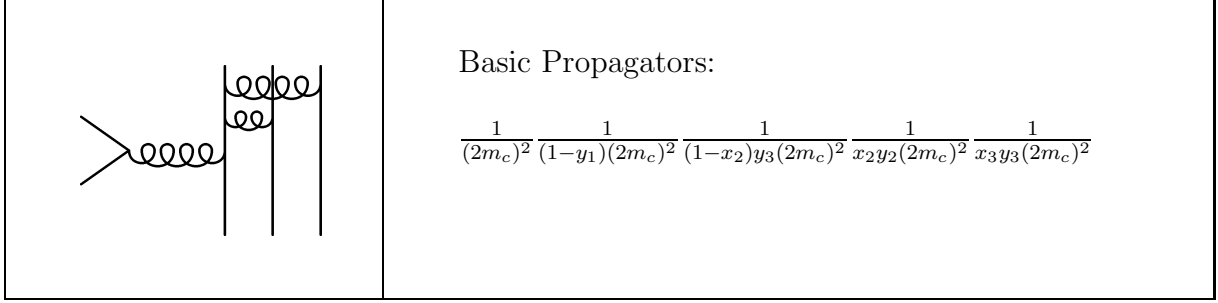


Figure 14: Basic graph of Group 7

A.7 Group 7

I.P.	Num. for graphs of Group 7 with $(\lambda_1, \lambda_2, \lambda_3)$			
	$(+, +, -)$		$(+, -, +)$	
	J=1	J=2	J=1	J=2
U3	$\frac{14\sqrt{2}}{27}(1-z)(x_3-z)(y_3-z)$		$-(-1)^J \frac{14\sqrt{2}}{27} z(1-x_2-z) \times (1-y_1-z)$	
L3	$\frac{32\sqrt{2}}{27}(1-z)(y_3-z)^2$		\emptyset	\emptyset
U2	$-\frac{40\sqrt{2}}{27}(1-z)(x_2-z)y_3$		\emptyset	\emptyset
L2	$\frac{32\sqrt{2}}{27}y_3\{(1-z)(y_2-z) + (-1)^J z(1-y_1-z)\}$		\emptyset	\emptyset
U1	$\frac{26\sqrt{2}}{27}(1-z)(x_1-z)(y_3-z)$		$(-1)^J \frac{26\sqrt{2}}{27} z(1-x_2-z) \times (1-y_1-z)$	
UM1	$-\frac{8\sqrt{2}}{27}y_3(1-z)(y_3-z)$		\emptyset	\emptyset
LM1	$-\frac{64\sqrt{2}}{27}y_3\{(1-z) - (-1)^J(1-y_1-z)\}$		\emptyset	\emptyset
L1	$-\frac{64\sqrt{2}}{27}y_3\{(y_1-z) + (-1)^J z\}$		\emptyset	\emptyset
G3	$-\frac{2\sqrt{2}}{3}(1-z)(x_3-y_3)(y_3-z)$		$(-1)^J \frac{\sqrt{2}}{3} (1-x_2-z) \times (1-y_1-z) \times (y_3+z)$	
G2	$-\frac{4\sqrt{2}}{3}y_3\{2(1-z)(x_2-y_2) - (-1)^J(x_2+z)(1-y_1-z)\}$		\emptyset	\emptyset

Table 11: (a) Numerators of the graphs of group 7 with helicity $(+, +, -)$ and $(+, -, +)$.

I.P.	Num. for graphs of Group 7 with ($\lambda_1, \lambda_2, \lambda_3$) = (-, +, +)		X-Prop.
	J=1	J=2	
U3	$-(-1)^J \frac{14\sqrt{2}}{27} z(1-x_2-z)(1-y_1-z)$		$\frac{1}{-z(x_3-z)(2m_c)^2}$
L3	\emptyset	\emptyset	$\frac{1}{-z(y_3-z)(2m_c)^2}$
U2	\emptyset	\emptyset	$\frac{1}{-z(x_2-z)(2m_c)^2}$
L2	$(-1)^J \frac{32\sqrt{2}}{27} zy_3(1-y_1-z)$		$\frac{1}{-z(y_2-z)(2m_c)^2}$
U1	\emptyset	\emptyset	$\frac{1}{-z(x_1-z)(2m_c)^2}$
UM1	$-(-1)^J \frac{8\sqrt{2}}{27} y_3(1-x_2-z)(1-y_1-z)$		$\frac{1}{(1-x_2)y_3(2m_c)^2}$
LM1	\emptyset	\emptyset	$\frac{1}{(1-y_1)(2m_c)^2}$
L1	\emptyset	\emptyset	$\frac{1}{-z(y_1-z)(2m_c)^2}$
G3	$(-1)^J \frac{\sqrt{2}}{3} (1-x_2-z)(1-y_1-z)(y_3+z)$		$\frac{1}{x_3y_3(2m_c)^2}$
G2	$(-1)^J \frac{4\sqrt{2}}{3} y_3(1-y_1-z)(x_2+z)$		$\frac{1}{x_2y_2(2m_c)^2}$

Table 11: (b) Numerators and the additional propagators of the graphs of group 7 with helicity (-,+,+).

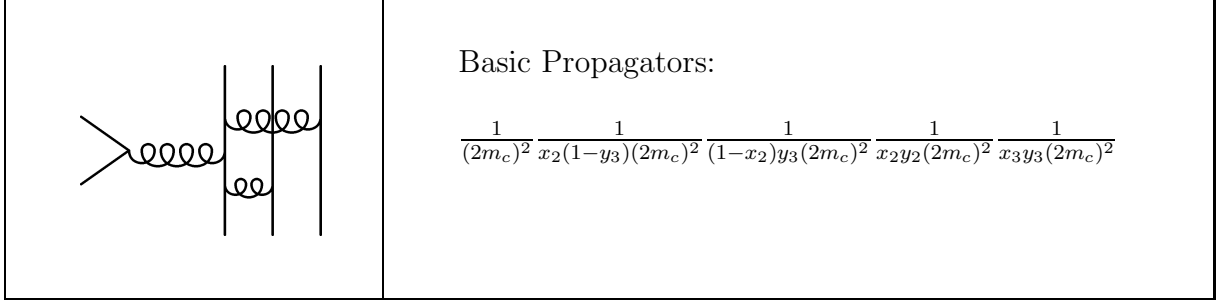


Figure 15: Basic graph of Group 8

A.8 Group 8

I.P.	Num. for graphs of Group 8 with $(\lambda_1, \lambda_2, \lambda_3)$			
	(+, +, -)		(+, -, +)	
	J=1	J=2	J=1	J=2
U3	\emptyset	\emptyset	$(-1)^J \frac{40\sqrt{2}}{27} x_2 z (1 - x_2 - z)$	
L3	\emptyset	\emptyset	\emptyset	\emptyset
U2	\emptyset	\emptyset	\emptyset	\emptyset
L2	$(-1)^J \frac{40\sqrt{2}}{27} y_3 z (1 - y_3 - z)$		\emptyset	\emptyset
U1	\emptyset	\emptyset	$(-1)^J \frac{8\sqrt{2}}{27} x_2 z (1 - x_2 - z)$	
UM1	\emptyset	\emptyset	\emptyset	\emptyset
LM1	\emptyset	\emptyset	\emptyset	\emptyset
L1	$(-1)^J \frac{8\sqrt{2}}{27} y_3 z (1 - y_3 - z)$		\emptyset	\emptyset
G3	\emptyset	\emptyset	$(-1)^J \frac{4\sqrt{2}}{3} x_2 (1 - x_2 - z) (y_3 + z)$	
G2	$(-1)^J \frac{4\sqrt{2}}{3} y_3 (1 - y_3 - z) (x_2 + z)$		\emptyset	\emptyset

Table 12: (a) Numerators of the graphs of group 8 with helicity (+,+,−) and (+,−,+).

I.P.	Num. for graphs of Group 8 with ($\lambda_1, \lambda_2, \lambda_3$) = (-, +, +)		X-Prop.
	J=1	J=2	
U3	$\frac{40\sqrt{2}}{27}x_2\{(x_3 - z)(y_3 - z) + (-1)^J z(1 - x_2 - z)\}$		$\frac{1}{-z(x_3 - z)(2m_c)^2}$
L3	$-\frac{32\sqrt{2}}{27}x_2(y_3 - z)^2$		$\frac{1}{-z(y_3 - z)(2m_c)^2}$
U2	$-\frac{32\sqrt{2}}{27}y_3(x_2 - z)^2$		$\frac{1}{-z(x_2 - z)(2m_c)^2}$
L2	$\frac{40\sqrt{2}}{27}y_3\{(x_2 - z)(y_2 - z) + (-1)^J z(1 - y_3 - z)\}$		$\frac{1}{-z(y_2 - z)(2m_c)^2}$
U1	$-\frac{8\sqrt{2}}{27}x_2(x_1 - z)(y_3 - z)$		$\frac{1}{-z(x_1 - z)(2m_c)^2}$
UM1	$-\frac{64\sqrt{2}}{27}x_2y_3\{(y_3 - z) - (-1)^J(1 - x_2 - z)\}$		$\frac{1}{(1 - x_2)y_3(2m_c)^2}$
LM1	$-\frac{64\sqrt{2}}{27}x_2y_3\{(x_2 - z) - (-1)^J(1 - y_3 - z)\}$		$\frac{1}{x_2(1 - y_3)(2m_c)^2}$
L1	$-\frac{8\sqrt{2}}{27}y_3(x_2 - z)(y_1 - z)$		$\frac{1}{-z(y_1 - z)(2m_c)^2}$
G3	$\frac{4\sqrt{2}}{3}x_2\{2(x_3 - y_3)(y_3 - z) + (-1)^J(1 - x_2 - z)(y_3 + z)\}$		$\frac{1}{x_3y_3(2m_c)^2}$
G2	$-\frac{4\sqrt{2}}{3}y_3\{2(x_2 - y_2)(x_2 - z) - (-1)^J(1 - y_3 - z)(x_2 + z)\}$		$\frac{1}{x_2y_2(2m_c)^2}$

Table 12: (b) Numerators and the additional propagators of the graphs of group 8 with helicity (-,+,+).

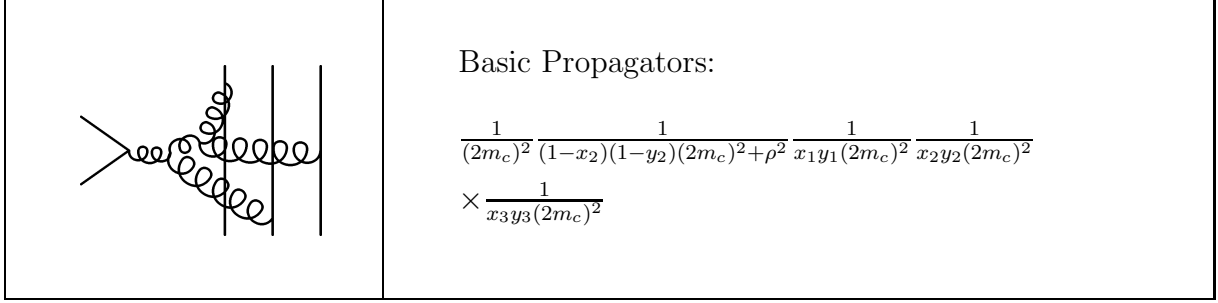


Figure 16: Basic graph of Group 9

A.9 Group 9

I.P.	Num. for graphs of Group 9 with $(\lambda_1, \lambda_2, \lambda_3)$			
	(+, +, -)		(+, -, +)	
	J=1	J=2	J=1	J=2
U3	$-\frac{1}{\sqrt{2}}(x_3 - z) \{ (1 + x_2 - z)(y_1 - y_3 + z) + (1 + y_2 - z)(x_1 - x_3 + z) \}$		$(-1)^J \sqrt{2} z (x_2 - y_2)(2x_1 + x_3 - z)$	
L3	$-\frac{1}{\sqrt{2}}(y_3 - z) \{ (1 + x_2 - z)(y_1 - y_3 + z) + (1 + y_2 - z)(x_1 - x_3 + z) \}$		$(-1)^J \sqrt{2} z (y_2 - x_2)(2y_1 + y_3 - z)$	
U2	\emptyset	\emptyset	\emptyset	\emptyset
L2	\emptyset	\emptyset	\emptyset	\emptyset
U1	$-\sqrt{2} \{ \frac{1}{2}(x_1 - z)[(1 + x_2 - z)(y_3 - y_1 + z) + (1 + y_2 - z)(x_3 - x_1 + z)] - (-1)^J z (x_2 - y_2)(2x_3 + x_1 - z) \}$		$(-1)^J \sqrt{2} z (x_2 - y_2)(2x_3 + x_1 - z)$	
L1	$-\sqrt{2} \{ \frac{1}{2}(y_1 - z)[(1 + x_2 - z)(y_3 - y_1 + z) + (1 + y_2 - z)(x_3 - x_1 + z)] - (-1)^J z (y_2 - x_2)(2y_3 + y_1 - z) \}$		$(-1)^J \sqrt{2} z (y_2 - x_2)(2y_3 + y_1 - z)$	
G3	\emptyset	\emptyset	\emptyset	\emptyset
G2	\emptyset	\emptyset	\emptyset	\emptyset
G1	\emptyset	\emptyset	\emptyset	\emptyset
GR	\emptyset	\emptyset	\emptyset	\emptyset
4G1	\emptyset	\emptyset	\emptyset	\emptyset
4G2	\emptyset	\emptyset	\emptyset	\emptyset

Table 13: (a) Numerators of the graphs of group 9 with helicity (+, +, -) and (+, -, +).

I.P.	Num. for graphs of Group 9 with ($\lambda_1, \lambda_2, \lambda_3$) = (-, +, +)		X-Prop.
	J=1	J=2	
U3	$-\sqrt{2}\left\{\frac{1}{2}(x_3 - z)\left[(1 + x_2 - z)(y_1 - y_3 + z) + (1 + y_2 - z)(x_1 - x_3 + z)\right] - (-1)^J z(x_2 - y_2)(2x_1 + x_3 - z)\right\}$		$\frac{1}{-z(x_3 - z)(2m_c)^2}$
L3	$-\sqrt{2}\left\{\frac{1}{2}(y_3 - z)\left[(1 + x_2 - z)(y_1 - y_3 + z) + (1 + y_2 - z)(x_1 - x_3 + z)\right] - (-1)^J z(y_2 - x_2)(2y_1 + y_3 - z)\right\}$		$\frac{1}{-z(y_3 - z)(2m_c)^2}$
U2	\emptyset	\emptyset	n. g.
L2	\emptyset	\emptyset	n. g.
U1	$-\frac{1}{\sqrt{2}}(x_1 - z)\left\{(1 + x_2 - z)(y_3 - y_1 + z) + (1 + y_2 - z)(x_3 - x_1 + z)\right\}$		$\frac{1}{-z(x_1 - z)(2m_c)^2}$
L1	$-\frac{1}{\sqrt{2}}(y_1 - z)\left\{(1 + x_2 - z)(y_3 - y_1 + z) + (1 + y_2 - z)(x_3 - x_1 + z)\right\}$		$\frac{1}{-z(y_1 - z)(2m_c)^2}$
G3	\emptyset	\emptyset	n. g.
G2	\emptyset	\emptyset	n. g.
G1	\emptyset	\emptyset	n. g.
GR	\emptyset	\emptyset	n. g.
4G1	\emptyset	\emptyset	none
4G2	\emptyset	\emptyset	none

Table 13: (b) Numerators and the additional propagators of the graphs of group 9 with helicity (-,+,+).

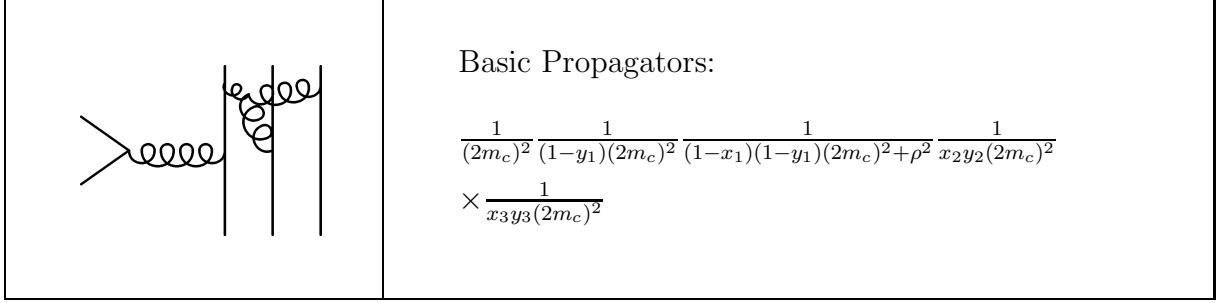


Figure 17: Basic graph of Group 10

A.10 Group 10

I.P.	Num. for graphs of Group 10 with $(\lambda_1, \lambda_2, \lambda_3)$			
	$(+, +, -)$		$(+, -, +)$	
	J=1	J=2	J=1	J=2
U3	$\sqrt{2}(1-z)(x_3-z)(y_3-y_2-z)$		$\sqrt{2}\{(1-z)(x_3-z)(y_3-y_2-z) + (-1)^J z(y_2+y_3-z)(2x_2+x_3-z)\}$	
L3	\emptyset	\emptyset	\emptyset	\emptyset
U2	$\sqrt{2}\{(1-z)(x_2-z)(y_2-y_3-z) + (-1)^J z(y_2+y_3-z)(2x_3+x_2-z)\}$		$\sqrt{2}(1-z)(x_2-z)(y_2-y_3-z)$	
L2	\emptyset	\emptyset	\emptyset	\emptyset
U1	\emptyset	\emptyset	\emptyset	\emptyset
M1	\emptyset	\emptyset	\emptyset	\emptyset
L1	\emptyset	\emptyset	\emptyset	\emptyset
G3	$\sqrt{2}(1-z)(x_3-y_3)(y_3-y_2-z)$		$\sqrt{2}\{(1-z)(x_3-y_3)(y_3-y_2-z) + (-1)^J (y_2+y_3-z) \times (x_3 y_2 + x_2 y_3 + x_3 y_3 + z(x_2+y_2-z))\}$	
G2	$\sqrt{2}\{(1-z)(x_2-y_2)(y_2-y_3-z) + (-1)^J (y_2+y_3-z) \times (x_3 y_2 + x_2 y_3 + x_2 y_2 + z(x_3+y_3-z))\}$		$\sqrt{2}(1-z)(x_2-y_2)(y_2-y_3-z)$	
GR	\emptyset	\emptyset	\emptyset	\emptyset
4G	$\sqrt{2}\{2(1-z) - (-1)^J (y_2+y_3-z)\}$		$\sqrt{2}\{2(1-z) - (-1)^J (y_2+y_3-z)\}$	

Table 14: (a) Numerators of the graphs of group 10 with helicity $(+, +, -)$ and $(+, -, +)$.

I.P.	Num. for graphs of Group 10 with ($\lambda_1, \lambda_2, \lambda_3$) = (-, +, +)		X-Prop.
	J=1	J=2	
U3	$(-1)^J \sqrt{2} z (y_2 + y_3 - z) (2x_2 + x_3 - z)$		$\frac{1}{-z(x_3-z)(2m_c)^2}$
L3	\emptyset	\emptyset	n. g.
U2	$(-1)^J \sqrt{2} z (y_2 + y_3 - z) (2x_3 + x_2 - z)$		$\frac{1}{-z(y_3-z)(2m_c)^2}$
L2	\emptyset	\emptyset	n. g.
U1	\emptyset	\emptyset	n. g.
M1	\emptyset	\emptyset	n. g.
L1	\emptyset	\emptyset	n. g.
G3	$(-1)^J \sqrt{2} (y_2 + y_3 - z) \times (x_3 y_2 + x_2 y_3 + x_3 y_3 + z(x_2 + y_2 - z))$		$\frac{1}{x_3 y_3 (2m_c)^2}$
G2	$(-1)^J \sqrt{2} (y_2 + y_3 - z) \times (x_3 y_2 + x_2 y_3 + x_2 y_2 + z(x_3 + y_3 - z))$		$\frac{1}{x_2 y_2 (2m_c)^2}$
GR	\emptyset	\emptyset	n. g.
4G	$(-1)^J 2\sqrt{2} (y_2 + y_3 - z)$		$\frac{1}{(2m_c)^2}$

Table 14: (b) Numerators and the additional propagators of the graphs of group 10 with helicity (-,+,+).

B Numerical Parameters

Here we gather together our input as well as other parameters used in the calculations in table form.

B.1 Basic Parameters

Symbol	Value
Λ_{QCD}	0.22 GeV
m_c	1.50 GeV
μ_0	1.00 GeV
μ_R (SHSA)	m_c
μ_R (MHSA)	square root of the largest virtuality, see section 6
n_f	4

Table 15: Basic input parameters.

B.2 Charmonium Parameters

Symbol	Value	Origin
$ R'_P(0) $	0.220 GeV ^{5/2}	see ref. [20, 37]
$f_{\chi_1}^{(8)}$	0.225×10^{-3} GeV ²	<i>obtained from fit here</i>
$f_{\chi_2}^{(8)}$	0.900×10^{-3} GeV ²	from ref. [20]
$z = z_3$	0.150	from ref. [20, 21]
$z_1 = z_2 = (1 - z)/2$	0.425	from ref. [20, 21]

Table 16: Charmonium parameters.

B.3 Baryon Wavefunction Parameters

Baryon	B_1	B_2	B_3	B_4	B_5
N	0.750	0.250	0.000	0.000	0.000
Σ	0.216	0.394	-0.293	-0.914	0.241
Ξ	1.106	0.050	-0.282	1.717	-0.498
Λ	-0.721	0.389	-0.150	-0.574	0.093
Δ	0.000	0.000	0.000	0.000	0.000
Σ^*	-0.547	0.182	-0.216	-1.081	0.062
Ξ^*	0.540	-0.180	-0.382	1.742	-0.413

Table 17: Baryon wavefunction parameters derived in ref. [11] with the constituent strange quark mass $m_s = 350$ MeV, the octet baryon decay constant $f_{B_8} = 6.64 \times 10^{-3}$ GeV² and the transverse size parameter $a_{B_8} = 0.75$ GeV⁻¹ at the reference scale μ_0 . The same for the decuplet baryons are $f_{B_{10}} = 0.0143$ GeV² and $a_{B_{10}} = 0.80$ GeV⁻¹. Note that in ref. [11] of all the decuplet baryons, only the parameters of Δ were given.

From these parameters, the mean-squared internal transverse momentum of the baryons $\rho^2 = \langle \mathbf{k}_\perp^2 \rangle$ can be worked out. The average value is $\rho_{(8)} = 415.0$ MeV for the octet and $\rho_{(10)} = 389.0$ MeV for the decuplet baryons. Their use as infrared cutoff was discussed in section 8.

References

- [1] S.J. Brodsky and G.P. Lepage, Phys. Rev. D **22**, 2157 (1980).
- [2] A. Duncan and A.H. Mueller, Phys. Lett. B **93**, 119 (1980).
- [3] G.T. Bodwin, E. Braaten and G.P. Lepage, Phys. Rev. D **46**, 1914 (1992).
- [4] G.T. Bodwin, E. Braaten and G.P. Lepage, Phys. Rev. D **51**, 1125 (1995).
- [5] V.L. Chernyak and A.R. Zhitnitsky, Nucl. Phys. B **201**, 492 (1982).
- [6] V.L. Chernyak and A.R. Zhitnitsky, Phys. Rep. **112**, 173 (1984).
- [7] V.L. Chernyak, A.A. Ogloblin and A.R. Zhitnitsky, Z. Phys. C **42**, 569 (1989).
- [8] J. Bolz, R. Jakob, P. Kroll, M. Bergmann and N.G. Stefanis, Z. Phys. C **66**, 267 (1995).
- [9] A.V. Radyushkin, Nucl. Phys. A **532**, 141 (1991).
- [10] J. Bolz and P. Kroll, Z. Phys. A **356**, 327 (1996).
- [11] J. Bolz and P. Kroll, Eur. Phys. J. C **2**, 454 (1998).
- [12] J. Botts and G. Sterman, Nucl. Phys. B **325**, 62 (1989).
- [13] H.N. Li and G. Sterman, Nucl. Phys. B **381**, 129 (1992).
- [14] S.M.H. Wong, preprint NUC-MINN-98/11-T, hep-ph/9903221.
- [15] M. Gari and N.G. Stefanis, Phys. Rev. D **35**, 1074 (1987).
- [16] I.D. King and C.T. Sachrajda, Nucl. Phys. B **279**, 785 (1987).
- [17] M. Bergmann and N.G. Stefanis, Phys. Rev. D **47**, 3685 (1993).
- [18] Z. Dziembowski, Phys. Rev. D **37**, 768 (1988).
- [19] S.J. Brodsky and G.P. Lepage, Phys. Rev. D **24**, 2848 (1981).
- [20] J. Bolz, P. Kroll and G.A. Schuler, Phys. Lett. B **392**, 198 (1997).
- [21] J. Bolz, P. Kroll and G.A. Schuler, Eur. Phys. J. C **2**, 705 (1998).
- [22] F. Murgia and M. Melis, Phys. Rev. D **54**, 3365 (1996).
- [23] R.M. Barnett et al, Phys. Rev. D **54**, 1 (1996).

- [24] A. Andrikopoulou, *Z. Phys. C* **22**, 63 (1984).
- [25] P.H. Damgaard, K. Tsokos and E.L. Berger, *Nucl. Phys. B* **259**, 285 (1985).
- [26] V.L. Chernyak, A.A. Ogloblin and A.R. Zhitnitsky, *Z. Phys. C* **42**, 583 (1989).
- [27] F. Murgia and M. Melis, *Phys. Rev. D* **51**, 3487 (1995).
- [28] V.A. Novikov, L.B. Okun, M.A. Shifman, A.I. Vainshtein, M.B. Voloshin and V.I. Zakharov, *Phys. Rep.* **41**, 1 (1978).
- [29] J.Z. Bai et al, BES Collaboration, *Phys. Rev. Lett.* **81**, 3091 (1998).
- [30] P. Kroll and S.M.H. Wong, in *Proceedings of the IVth International Workshop on Progress in Heavy Quark Physics, Rostock, Germany, 1997*, edited by M. Beyer, T. Mannel and H. Schröder (Rostock University Press, 1998), p. 185.
- [31] G. Grunberg, *Phys. Lett. B* **327**, 121 (1996).
- [32] Yu.L. Dokshitzer, V.A. Khoze, and S.I. Troyan, *Phys. Rev. D* **53**, 89 (1996).
- [33] D.V. Shirkov and I.L. Solovtsov, *Phys. Rev. Lett.* **79**, 1209 (1997).
- [34] B.R. Webber, *JHEP* **10**, 012 (1998).
- [35] S.M.H. Wong, work in progress.
- [36] H.Ch. Kim, W. Schroers and N.G. Stefanis, preprint RUB-TPII-17/98, PNU-NTG-04/98, hep-ph/9812280.
- [37] M.L. Mangano and A. Petrelli, *Phys. Lett. B* **352**, 445 (1995).

Figure Captions

- 1) Basic graphs that could contribute to χ_J colour singlet decay. But actually, only graphs of type (a) can contribute.
- 2) Graphs of type Fig. 1 (a) can be divided further into four groups.
- 3) In addition to the graphs of type Fig. 1, these form the bases of further contributions in the colour octet decay channel.
- 4) Our labelling scheme as applied to (a) Group 2 and (b) Group 4.
- 5) Examples of complete colour octet graphs. (a) graph U1 and (b) graph L2 of Group 5, and (c) graph L3 of Group 1.
- 6) Examples of complete colour octet graphs with 4-gluon vertex. (a) graph 4G of Group 4 and (b) graph 4G of Group 10.
- 7) Basic graph of Group 1
- 8) Basic graph of Group 2
- 9) Basic graph of Group 2'
- 10) Basic graph of Group 3
- 11) Basic graph of Group 4
- 12) Basic graph of Group 5
- 13) Basic graph of Group 6
- 14) Basic graph of Group 7
- 15) Basic graph of Group 8
- 16) Basic graph of Group 9
- 17) Basic graph of Group 10

Table Captions

- 1) The expansion coefficients of the distribution amplitudes $\phi_{123}^{B_{10}}$ of the octet baryons considered in the χ_J decay. The parameters associated with this set of coefficients are $f_{B_{10}}(\mu_0) = 0.0143 \text{ GeV}^2$ and $a_{B_{10}} = 0.80 \text{ GeV}^{-1}$.
- 2) Clearly, the colour singlet contributions are insufficient in explaining the experimental data of χ_J decay into $p\bar{p}$.
- 3) The partial decay widths for χ_J decay into octet and decuplet baryon-antibaryon pairs. The width of $\chi_1 \rightarrow N\bar{N}$ in parenthesis is to indicate that this value is a fit unlike all partial widths of χ_2 which are predictions. Based on this fit, the rest of χ_1 widths are also predictions.
- 4) Comparing our results with the measured widths from the PDG [23] data and from the BES collaboration [29]. This branching ratio of χ_1 is a fit.
- 5a) Numerators of the graphs of group 1 with helicity $(+,+,-)$.
- 5b) Numerators of the graphs of group 1 with helicity $(+,-,+)$.
- 5c) Numerators and the additional propagators of the graphs of group 1 with helicity $(-,+,+)$.
- 6a) Numerators of the graphs of group 2 with helicity $(+,+,-)$ and $(+,-,+)$.
- 6b) Numerators and the additional propagators of the graphs of group 2 with helicity $(-,+,+)$.
- 6a') Numerators of the graphs of group 2' with helicity $(+,+,-)$.
- 6b') Numerators of the graphs of group 2' with helicity $(+,-,+)$.
- 6c') Numerators and the additional propagators of the graphs of group 2' with helicity $(-,+,+)$.
- 7a) Numerators of the graphs of group 3 with helicity $(+,+,-)$.
- 7b) Numerators of the graphs of group 3 with helicity $(+,-,+)$.
- 7c) Numerators and the additional propagators of the graphs of group 3 with helicity $(-,+,+)$.
- 8a) Numerators of the graphs of group 4 with helicity $(+,+,-)$ and $(+,-,+)$.
- 8b) Numerators and the additional propagators of the graphs of group 4 with helicity $(-,+,+)$.

- 9a) Numerators of the graphs of group 5 with helicity $(+,+,-)$.
- 9b) Numerators of the graphs of group 5 with helicity $(+,-,+)$.
- 9c) Numerators and the additional propagators of the graphs of group 5 with helicity $(-,+,+)$.
- 10a) Numerators of the graphs of group 6 with helicity $(+,+,-)$ and $(+,-,+)$.
- 10b) Numerators and the additional propagators of the graphs of group 6 with helicity $(-,+,+)$.
- 11a) Numerators of the graphs of group 7 with helicity $(+,+,-)$ and $(+,-,+)$.
- 11b) Numerators and the additional propagators of the graphs of group 7 with helicity $(-,+,+)$.
- 12a) Numerators of the graphs of group 8 with helicity $(+,+,-)$ and $(+,-,+)$.
- 12b) Numerators and the additional propagators of the graphs of group 8 with helicity $(-,+,+)$.
- 13a) Numerators of the graphs of group 9 with helicity $(+,+,-)$ and $(+,-,+)$.
- 13b) Numerators and the additional propagators of the graphs of group 9 with helicity $(-,+,+)$.
- 14a) Numerators of the graphs of group 10 with helicity $(+,+,-)$ and $(+,-,+)$.
- 14b) Numerators and the additional propagators of the graphs of group 10 with helicity $(-,+,+)$.
- 15) Basic input parameters.
- 16) Charmonium parameters.
- 17) Baryon wavefunction parameters derived in ref. [11] with the constituent strange quark mass $m_s = 350$ MeV, the octet baryon decay constant $f_{B_8} = 6.64 \times 10^{-3}$ GeV² and the transverse size parameter $a_{B_8} = 0.75$ GeV⁻¹ at the reference scale μ_0 . The same for the decuplet baryons are $f_{B_{10}} = 0.0143$ GeV² and $a_{B_{10}} = 0.80$ GeV⁻¹. Note that in ref. [11] of all the decuplet baryons, only the parameters of Δ were given.